INSTITUTO NACIONAL DE MATEMÁTICA PURA E APLICADA

# A REDUCED MODEL FOR INTERNAL WAVES INTERACTING WITH SUBMARINE STRUCTURES AT INTERMEDIATE DEPTH

Author: Ailín Ruiz de Zárate Fábregas

Adviser: Prof. Dr. André Nachbin

2007






*To my family*

# Acknowledgements

First, I would like to thank Professor Nachbin for his support, encouragement and guidance along these years and for introducing me to the fascinating world of water waves. It has been a privilege to work with him.

It has been also a pleasure to study at IMPA, for the institution provides all the conditions for it. In particular, the Fluid Dynamics Group at IMPA has developed an excellent atmosphere for work.

I appreciate the effort of my teachers in Brazil and in Cuba. I owe them my best results, now and ever.

I would like to thank Professor Wooyoung Choi for his useful comments regarding this work and future extensions and Professor Uri Ascher for his observations about the stability of numerical schemes.

I would like to express my deepest gratitude to my husband, Rodrigo Morante, for his support, help and love along these years. Without him I would not have been able to complete this project. In particular, I thank him for helping me typing, generating part of the figures and correcting the work presented here.

I thank my Mom for have been always ready to help me, specially in the most difficult moments.

I thank my friends, they are few but very trustworthy.

I thank Professors Daniel Alfaro, Stefanella Boatto, Roberto Kraenkel, Dan Marchesin and Jorge Zubelli for kindly accepting to participate in my thesis committee.

I thank the ANP/PRH-32 scholarship program and CAPES for financial support.

# Contents

# Abstract

A reduced one-dimensional strongly nonlinear model for the evolution of internal waves over an arbitrary bottom topography is derived. The reduced model is aimed at obtaining an efficient numerical method for the two-dimensional problem. Two layers containing inviscid, immiscible, irrotational fluids of different densities are defined. The upper layer is shallow compared with the characteristic wavelength at the interface of the two-fluid system, while the depth of the bottom region is comparable to the characteristic wavelength. The nonlinear evolution equations obtained describe the behaviour of the internal wave elevation and mean upper-velocity for this water configuration. The system is a generalization of the one proposed by Choi and Camassa for the flat bottom case in the same physical settings. Due to the presence of topography a variable coefficient accompanies each space derivative. These Boussinesq-type equations contain the Intermediate Long Wave (ILW) equation and the Benjamin-Ono (BO) equation when restricted to the unidirectional wave regime. We intend to use this model to study the interaction of waves with the bottom profile. The dynamics include wave scattering, dispersion and attenuation among other phenomena. The research is relevant in oil recovery in deep ocean waters, where salt concentration and differences in temperature generate stratification in such a way that internal waves can affect offshore operations and submerged structures.

# Resumo

É obtido um modelo reduzido unidirecional fortemente não linear para a evolução de ondas internas sobre topografias de fundo arbitrário. Com o modelo reduzido busca-se obter métodos numéricos eficientes para resolver o problema bidimensional. São consideradas duas camadas contendo dois fluidos invíscidos, imiscíveis e irrotacionais de densidades diferentes. A camada superior é delgada se comparada à longitude de onda característica. As equações de evolução não lineares obtidas descrevem o comportamento da elevação da onda interna e a velocidade superior média para esta configuração da água. O sistema é uma generalização daquele proposto por Choi e Camassa para o caso de fundo plano nas mesmas condições físicas. Devido à presença da topografia, cada derivada espacial está acompanhada por um coeficiente variável. Estas equações de Boussinesq contêm a equação da Onda Longa Intermediária (*Intermediate Long Wave*, ILW) e a equação de Benjamin-Ono (BO) se restritas ao regime unidirecional de propagação de ondas. Pretendemos utilizar este modelo para estudar a interação das ondas com o perfil do fundo. A dinâmica inclui reflexão, dispersão e atenuação das ondas entre outros fenômenos. A pesquisa é de importância na recuperação de petróleo em águas profundas oceânicas onde a concentração de sal e as diferenças de temperatura geram estratificação de tal forma que as ondas internas podem afetar as operações *offshore* e as estruturas submersas.

# Chapter 1

# Introduction

Modelling waves is of great interest in the study of ocean dynamics. Internal ocean waves, for example, appear when salt concentration and differences in temperature generate stratification. They can interact with the bottom topography and submerged structures as well as with surface waves. In particular, in oil recovery in deep ocean waters, internal waves can affect offshore operations and submerged structures. Accurate reduced models are a first step in producing efficient computational methods for engineering problems in oceanography. This was the goal in [24, 1].

To describe this nonlinear wave phenomenon in deep waters there are several bidirectional models containing the Intermediate Long Wave (ILW) equation and the Benjamin-Ono (BO) equation, starting from works such as [3, 9, 25, 14, 17] to more recent papers such as [20, 6, 7, 8, 13]. In these models two fundamental mechanisms, nonlinearity and dispersion, are responsible for the main features of the propagating wave. One of the most interesting behaviours observed is the existence of solitary wave solutions with permanent shape. They are observed

when the steepening of a given wave front due to the nonlinearity and the attenuation and flattenning promoted by the dispersion are balanced on a particular scale. Usually the contribution of nonlinearity is quantified by the non-dimensional nonlinearity parameter $\alpha$, which is the ratio between the wave amplitude and the fluid layer thickness. It appears as a small non-zero parameter in the so-called weakly nonlinear regime, and accompanies the nonlinear terms. On the other hand, the dispersion parameter $\beta$ is the squared ratio between the fluid layer thickness and the typical wavelength. It appears in the dispersion relation, making the phase velocity a function of the wavenumber $k$. The balance that creates a solitary wave is commonly obtained through a scaling relation between $\alpha$ and $\beta$, in the form of a power law, for asymptotic values $\alpha \ll 1$ and $\beta \ll 1$. In the water configuration considered here, it is the scaling $\alpha = O(\sqrt{\beta})$ that leads to the ILW [14, 17]. In the limit when one layer thickness tends to infinity, the ILW equation becomes the BO equation [3, 9, 25].

For all these models, the dependence on the vertical coordinate has been eliminated by focusing on specific regimes and using systematic asymptotic expansion methods in small parameters. This results in a considerable simplification of the original Euler equations that leads to more efficient computational methods than the integration of the Euler system in the presence of a free interface. However, the approximation needs to be accurate even for large values of the parameters $\alpha$ and $\beta$. In other words, the model needs to be robust enough to cover several regimes in which the viscosity effects are negligible, justifying the use of the Euler equations. In [8], the authors compared weakly nonlinear models with experimental data obtained by Koop and Butler in [16]. They found a divergence. This motivated them to propose a strongly nonlinear model for flat bottom that shares

the simplicity of the weakly nonlinear ones and extends its domain of validity. The numerical results agree very well with the experimental data. This model is generalized in the present work to consider an arbitrary sea bottom. We also improve the asymptotic expansion to the next order of approximation in the pressure term by taking a nonhydrostatic correction term. The resulting strongly nonlinear model of higher order is more complicated than the previous one mentioned here, but it has a weakly nonlinear version very similar to the strongly nonlinear model of lower order. This fact implies that the weakly nonlinear higher-order model should serve as a good model for moderate amplitude internal waves in a deep water configuration. We remark that the new models support bidirectional wave propagation, so they are able to capture the reflected wave from the propagation over a nonuniform sea bottom.

The models found in the literature consider flat or slowly varying bottom topography. Here, the model of Choi and Camassa is generalized to the case of an arbitrary bottom topography by using the conformal mapping technique described in [24]. We obtained a strongly nonlinear long-wave model like Choi and Camassa's, which is able to describe large amplitude internal solitary waves. A system of two layers constrained to a region limited by a horizontal rigid lid at the top and an arbitrary bottom topography is considered, as described in Fig. 2.1. The upper layer is shallow compared with the characteristic wavelength at the interface of the two-fluid system, while the lower region is deeper. The nonlinear evolution equations describe the behaviour of the internal wave elevation and mean upper-velocity for this water configuration. These Boussinesq-type equations contain the ILW equation and the BO equation in the unidirectional wave regime. We intend to use this model to study the interaction of waves with the bottom profile,

in particular that of solitary waves. This is part of our future goals. The dynamics described include wave scattering, dispersion and attenuation among other phenomena.

The work is organized as follows. In Chapter 2 the physical setting is presented and as the main result, a reduced strongly nonlinear one-dimensional model is proposed. Section 2.1 is devoted to obtaining a set of upper layer averaged equations that will be completed with information provided by the lower layer in order to derive the reduced model. The continuity of pressure at the interface establishes a connection between both layers, as shown in Section 2.2. Through this condition we add the topography information to the averaged upper layer system. The case when the depth of the bottom layer approaches infinity is also considered. In Section 2.3 the dispersion relations for the linearized models are computed. An ILW equation with variable coefficient and the BO equation are obtained from the reduced models as unidirectional wave propagation models in Section 2.4. In Section 2.5 theoretical solitary wave solutions are presented for the ILW equation and for the Regularized ILW equation. The purpose of Chapter 3 is to exhibit a model that improves the order in the asymptotic approximation in the pressure term of the reduced model obtained in Chapter 2. To that end, in Section 3.1 one more term of the asymptotic expansion of the mean horizontal derivative of pressure is added to the upper layer averaged equations. Then, in Section 3.2, the approximation of the pressure at the interface is improved and a reduced strongly nonlinear one-dimensional model of higher-order is obtained. The dispersion relations for the higher-order model and for the previous model are compared with the full dispersion relation originating from the Euler equations in Section 3.3. Chapter 4 is devoted to the numerical resolution of the reduced model obtained

in Chapter 2. A hierarchy of one-dimensional models can be derived from this strongly nonlinear model as shown in Section 4.1 by considering the different regimes (linear, weakly nonlinear or strongly nonlinear) as well as the flat or corrugated bottom cases. Numerical schemes based on the method of lines for all models are described in Section 4.2 together with the study of their stability properties. The results from the Matlab implementations are shown in Sections 4.3, 4.4 and 4.5, including periodic topography experiments and solitary wave solutions. Technical justifications for the manipulations done in Section 2.4 are provided in Appendix A. The relation between the Hilbert transform on the strip (involved in the models considered) and the Dirichlet-to-Neumann operator is presented in Appendix B. Due to the nonlocal definition of the Hilbert transform on the strip, it must be redefined on the periodic domain used for numerical implementations, as done in Appendix C.

# Chapter 2

# Derivation of the reduced model

In this chapter we generalize the work by Choi and Camassa [8]. Their asymptotic technique for reducing a pair of two-dimensional (2D) systems of nonlinear partial differential equations (PDEs) to a single one-dimensional (1D) system of PDEs at an interface, is generalized to include very general submarine structures and topographies at the bottom of the lower fluid layer.

We start with a two-fluid configuration. Define the density of each inviscid, immiscible, irrotational fluid as $\rho_1$ for the upper layer and $\rho_2$ for the lower layer. For a stable stratification, $\rho_2 > \rho_1$. Similarly, $(u_i, w_i)$ denotes the velocity components and $p_i$ the pressure, where $i = 1, 2$. The upper layer is assumed to have an undisturbed thickness $h_1$, much smaller than the characteristic wavelength of the perturbed interface $L > 0$, hence the upper layer will be in the shallow water regime. At the lower layer the irregular bottom is described by $z = h_2(h(x/l) - 1)$. The function $h$ needs not to be continuous neither univalued, see for example Fig. 2.1 where a polygonal shaped topography is sketched. We can assume that $h$ has compact support so the roughness is confined to a finite interval. More-

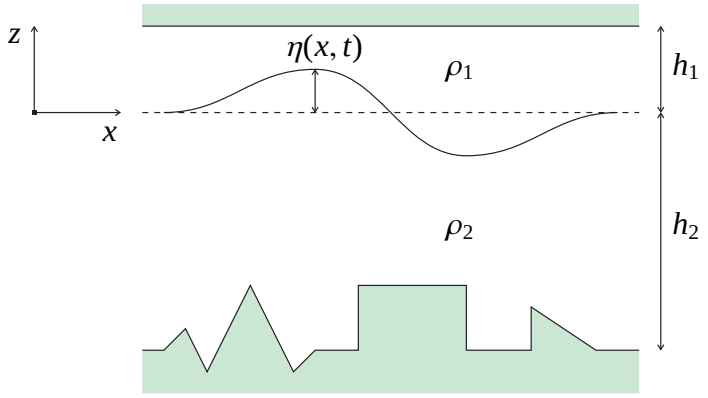


Figure 2.1: Two-fluid system configuration.

over $h_2$ is the undisturbed thickness of the lower layer outside the irregular bottom region and it is comparable with the characteristic wavelength $L$, that characterizes an intermediate depth regime. In the slowly varying bottom case we define $\varepsilon = L/l \ll 1$; when a more rapidly varying bottom is of concern, the horizontal length scale for bottom irregularities $l$ is such that $h_1 < l \ll L$. The coordinate system is positioned at the undisturbed interface between layers. The displacement of the interface is denoted by $\eta(x,t)$ and we may assume that initially it has compact support.

The corresponding Euler equations are

$$\begin{aligned} u_{ix} + w_{iz} &= 0, \\ u_{it} + u_i u_{ix} + w_i u_{iz} &= -\frac{p_{ix}}{\rho_i}, \\ w_{it} + u_i w_{ix} + w_i w_{iz} &= -\frac{p_{iz}}{\rho_i} - g, \end{aligned}$$

for $i = 1, 2$. Subscripts $x$, $z$ and $t$ stand for partial derivatives with respect to spatial coordinates and time. The continuity condition at the interface $z = \eta(x,t)$

demands that

$$\eta_t + u_i \eta_x = w_i, \qquad p_1 = p_2,$$

namely, a kinematic condition for the material curve and no pressure jumps allowed.

At the top we impose a rigid lid condition,

$$w_1(x, h_1, t) = 0,$$

commonly used in ocean and atmospheric models, while at the irregular impermeable bottom

$$-\frac{h_2}{l} h'\left(\frac{x}{l}\right) u_2 + w_2 = 0.$$

Introducing the dimensionless dispersion parameter $\beta = \left(\frac{h_1}{L}\right)^2$, it follows from the shallowness of the upper layer that

$$O\left(\sqrt{\beta}\right) = O\left(\frac{h_1}{L}\right) \ll 1.$$

From the continuity equation for $i = 1$ we have,

$$\frac{w_1}{u_1} = O\left(\frac{h_1}{L}\right) = O\left(\sqrt{\beta}\right).$$

Let $U_0 = \sqrt{g h_1}$ be the characteristic shallow layer speed. According to these scalings, physical variables involved in the upper layer equations are non-dimen-

sionalized as follows:

$$x = L\tilde{x}, \qquad z = h_1\tilde{z}, \qquad t = \frac{L}{U_0}\tilde{t}, \qquad \eta = h_1\tilde{\eta},$$
$$u_1 = U_0\tilde{u}_1, \qquad w_1 = \sqrt{\beta}U_0\tilde{w}_1, \qquad p_1 = (\rho_1 U_0^2)\tilde{p}_1.$$

In a weakly nonlinear theory, $\eta$ is usually scaled by a small parameter. Note that here we have an $O(1)$ scaling. This will lead to a strongly nonlinear model.

## 2.1 Reducing the upper layer dynamics to the interface

The dimensionless equations for the upper layer (the tilde has been removed) are:

$$\begin{aligned} u_{1x} + w_{1z} &= 0, \\ u_{1t} + u_1 u_{1x} + w_1 u_{1z} &= -p_{1x}, \\ \beta\,(w_{1t} + u_1 w_{1x} + w_1 w_{1z}) &= -p_{1z} - 1. \end{aligned} \tag{2.1}$$

The boundary conditions are

$$\begin{aligned} \eta_t + u_1\eta_x = w_1 \quad \text{and} \quad p_1 = p_2 \quad \text{at} \quad z = \eta(x,t), \\ w_1(x,1,t) = 0. \end{aligned} \tag{2.2}$$

Focusing on the upper shallow region, consider the following definition: for any

function $f(x,z,t)$, let its associated *mean-layer quantity* $\overline{f}$ be

$$\overline{f}(x,t) = \frac{1}{1-\eta}\int_{\eta}^{1} f(x,z,t)\ dz.$$

By averaging we will reduce the 2D Euler equations to a 1D system.

Let $\eta_1 = 1-\eta$. From the horizontal momentum equation we have

$$\eta_1\overline{u_{1t}} + \eta_1\overline{u_1 u_{1x}} + \eta_1\overline{w_1 u_{1z}} = -\eta_1\overline{p_{1x}}. \tag{2.3}$$

We need to express each of these mean-layer quantities in terms of $\overline{u_1}$ and $\eta$. The difficulty at this stage is breaking up the mean of square, and other general quadratic terms, into individually averaged terms. To begin with, note that

$$\begin{aligned}(\eta_1\overline{u_1})_t &= \int_{\eta}^{1} u_{1t}\ dz - \eta_t u_1(x,\eta,t),\\ &= \eta_1\overline{u_{1t}} - \eta_t u_1,\end{aligned}$$

where $u_1$ is evaluated at the interface $(x,z,t) = (x,\eta(x,t),t)$. So,

$$\eta_1\overline{u_{1t}} = (\eta_1\overline{u_1})_t + \eta_t u_1. \tag{2.4}$$

Similarly

$$\eta_1\overline{u_{1x}} = u_1\eta_x + (\eta_1\overline{u_1})_x, \tag{2.5}$$

and

$$2\eta_1\overline{u_1 u_{1x}} = \eta_x u_1^2 + \left(\eta_1\overline{u_1^2}\right)_x. \tag{2.6}$$

Therefore at $z = \eta(x,t)$,

$$\eta_1(\overline{u_{1t}} + \overline{u_1 u_{1x}}) = (\eta_1 \overline{u_1})_t + u_1\eta_t + \frac{1}{2}\eta_x u_1^2 + \frac{1}{2}\left(\eta_1 \overline{u_1^2}\right)_x .$$

From the kinematic condition Eq. (2.2)

$$u_1\eta_t + \frac{1}{2}\eta_x u_1^2 = u_1 w_1 - \frac{1}{2}\eta_x u_1^2,$$

and by substitution,

$$\eta_1(\overline{u_{1t}} + \overline{u_1 u_{1x}}) = (\eta_1 \overline{u_1})_t + u_1 w_1 - \frac{1}{2}\eta_x u_1^2 + \frac{1}{2}\left(\eta_1 \overline{u_1^2}\right)_x . \tag{2.7}$$

On the other hand, integration by parts and incompressibility give

$$\eta_1 \overline{w_1 u_{1z}} = -w_1 u_1 - \int_\eta^1 w_{1z} u_1 \, dz = -w_1 u_1 + \int_\eta^1 u_{1x} u_1 \, dz.$$

From Eq. (2.6),

$$\eta_1 \overline{w_1 u_{1z}} = -w_1 u_1 + \frac{1}{2}\eta_x u_1^2 + \frac{1}{2}\left(\eta_1 \overline{u_1^2}\right)_x . \tag{2.8}$$

Substituting Eqs. (2.7) and (2.8) in Eq. (2.3), the following mean-layer equation is derived

$$(\eta_1 \overline{u_1})_t + \left(\eta_1 \overline{u_1^2}\right)_x = -\eta_1 \overline{p_{1x}}. \tag{2.9}$$

The incompressibility condition gives $w_1 = \eta_1 \overline{u_{1x}}$ at $z = \eta(x,t)$. This, together with Eq. (2.5) shows that

$$w_1 = u_1\eta_x + (\eta_1 \overline{u_1})_x.$$

Substitution of $w_1$ into Eq. (2.2) leads to $\eta_t + u_1\eta_x = u_1\eta_x + (\eta_1\overline{u_1})_x$ and

$$-\eta_{1_t} = (\eta_1\overline{u_1})_x. \tag{2.10}$$

As pointed in [8], the system of Eqs. (2.9)–(2.10) was already considered in [31, 5] for surface waves. In reducing (averaging) the 2D Euler equations to this 1D system no approximations have been made up to this point. Nevertheless, the quantities $\overline{u_1 \cdot u_1}$ and $\overline{p_{1_x}}$ prevent the closure of the system of Eqs. (2.9)–(2.10). These quantities will be expressed in terms of $\eta$ and $\overline{u_1}$ up to a certain order in the dispersion parameter $\beta$. Note that until now, we still have not used the vertical momentum equation and the continuity of pressure boundary condition. We start by approximating $\overline{p_{1_x}}$ and then proceed to do the same for $\overline{u_1 \cdot u_1}$.

The vertical momentum equation over a shallow layer suggests the following asymptotic expansion in powers of $\beta$

$$f(x, z, t) = f^{(0)} + \beta f^{(1)} + O(\beta^2)$$

for any of the functions $u_1$, $w_1$, $p_1$. In fact, from Eq. (2.1), $p_{1_z} = -1 + O(\beta)$. Integrating from $\eta$ to $z$ we have that

$$p_1(x, z, t) - p_1(x, \eta, t) = -(z - \eta) + O(\beta),$$

and the pressure continuity across the interface gives

$$p_1(x, z, t) = p_2(x, \eta, t) - (z - \eta) + O(\beta).$$

The pressure $p_2(x, \eta, t)$ should be non-dimensionalized in the same fashion as $p_1$, that is,

$$p_2 = \rho_1 U_0^2 \tilde{p}_2.$$

Define $P(x, t) = p_2(x, \eta(x, t), t)$. Then

$$p_1 = P(x, t) - (z - \eta) + O(\beta),$$

which immediately yields

$$p_{1x} = P_x(x, t) + \eta_x + O(\beta).$$

By averaging we get

$$\begin{aligned} \overline{p_{1x}} &= \frac{1}{\eta_1} \int_{\eta}^{1} P_x(x, t)\ dz + \eta_x + O(\beta), \\ &= P_x(x, t) + \eta_x + O(\beta), \\ &= \Big( p_2(x, \eta(x, t), t) \Big)_x + \eta_x + O(\beta). \end{aligned} \tag{2.11}$$

An approximation for $P_x$ will be obtained later from the Euler equations for the lower fluid layer. We now approximate the mean squared horizontal velocity in terms of $\overline{u_1}$ and $\eta$.

In order to express $\overline{u_1 \cdot u_1}$ as a function of $\overline{u_1}$ and $\eta$, it should be pointed out that the irrotational condition in non-dimensional variables is

$$\frac{U_0}{h_1} u_{1z} = \sqrt{\beta} \frac{U_0}{L} w_{1x},$$

i. e. $u_{1z} = \beta w_{1x}$. Hence $\left(u_1^{(0)}\right)_z = 0$ and as expected for shallow water flows $u_1^{(0)}$ is independent from $z$:

$$u_1^{(0)} = u_1^{(0)}(x, t). \tag{2.12}$$

We now correct this first order approximation. By using

$$u_1 = u_1^{(0)} + \beta u_1^{(1)} + O(\beta^2) \tag{2.13}$$

and Eq. (2.12) it is straightforward that

$$u_1^2 = {u_1^{(0)}}^2 + 2\beta u_1^{(1)} u_1^{(0)} + O(\beta^2),$$

$$\int_\eta^1 u_1^2 \, dz = \int_\eta^1 {u_1^{(0)}}^2 \, dz + 2\beta \int_\eta^1 u_1^{(1)} u_1^{(0)} \, dz + O(\beta^2),$$

and

$$\eta_1 \overline{u_1 \cdot u_1} = {u_1^{(0)}}^2 (1 - \eta) + 2\eta_1 \beta u_1^{(0)} \overline{u_1^{(1)}} + O(\beta^2),$$

so that

$$\overline{u_1 \cdot u_1} = u_1^{(0)} \cdot u_1^{(0)} + 2\beta u_1^{(0)} \overline{u_1^{(1)}} + O(\beta^2). \tag{2.14}$$

Also from Eq. (2.13),

$$\frac{1}{\eta_1} \int_\eta^1 u_1 \, dz = u_1^{(0)} + \beta \overline{u_1^{(1)}} + O(\beta^2),$$

$$\overline{u_1} = u_1^{(0)} + \beta \overline{u_1^{(1)}} + O(\beta^2),$$

$$\overline{u_1} \cdot \overline{u_1} = u_1^{(0)} \cdot u_1^{(0)} + 2\beta u_1^{(0)} \overline{u_1^{(1)}} + O(\beta^2). \tag{2.15}$$

Thus Eqs. (2.14) and (2.15) lead to our desired approximation, namely that

$$\eta_1 \overline{u_1 \cdot u_1} = \eta_1 \overline{u_1} \cdot \overline{u_1} + O(\beta^2). \tag{2.16}$$

Using Eq. (2.16), the nonlinear interfacial system (2.9) becomes

$$\eta_{1_t} \overline{u_1} + \eta_1 \overline{u_{1_t}} + (\eta_1 \overline{u_1} \cdot \overline{u_1} + O(\beta^2))_x = -\eta_1 \overline{p_{1_x}},$$
$$\eta_{1_t} \overline{u_1} + \eta_1 \overline{u_{1_t}} + \overline{u_1}(\eta_1 \overline{u_1})_x + \eta_1 \overline{u_1} \cdot \overline{u_{1_x}} = -\eta_1 \overline{p_{1_x}} + O(\beta^2).$$

From Eq. (2.10) one obtains that

$$\eta_1 \overline{u_{1_t}} + \eta_1 \overline{u_1} \cdot \overline{u_{1_x}} = -\eta_1 \overline{p_{1_x}} + O(\beta^2). \tag{2.17}$$

After substitution of Eq. (2.11), the following set of approximate equations for the upper layer was derived from Eqs. (2.9), (2.10):

$$\eta_{1_t} + (\eta_1 \overline{u_1})_x = 0,$$
$$\overline{u_{1_t}} + \overline{u_1} \cdot \overline{u_{1_x}} = -\eta_x - \Big(p_2(x, \eta(x,t), t)\Big)_x + O(\beta),$$

or equivalently,

$$\begin{cases} -\eta_t + ((1-\eta)\overline{u_1})_x = 0, \\ \overline{u_{1_t}} + \overline{u_1} \cdot \overline{u_{1_x}} = -\eta_x - \Big(p_2(x, \eta(x,t), t)\Big)_x + O(\beta). \end{cases} \tag{2.18}$$

We have almost closed our system of PDEs. Now we need to get an expression for $p_2$ in order to close the system and also to establish a connection with the lower

fluid layer.

## 2.2 Connecting the upper and lower layers

The coupling of the upper and lower layers is done through the pressure term. To get an approximation for $P_x(x,t) = \Big(p_2(x,\eta(x,t),t)\Big)_x$ from the Euler equations for the lower fluid layer, notice that out of the shallow water approximation

$$\frac{h_2}{L} = O(1),$$

so that the following scaling relation

$$\frac{w_2}{u_2} = O\left(\frac{h_2}{L}\right) = O(1)$$

follows from the continuity equation. At the interface, from the kinematic conditions and the relations above, we have that

$$\frac{w_2}{u_1} = O\left(\sqrt{\beta}\right), \qquad \frac{u_2}{u_1} = O\left(\sqrt{\beta}\right),$$

at $z = \eta$. Following these scalings introduce the dimensionless variables for the lower region (with a tilde)

$$x = L\tilde{x}, \qquad z = L\tilde{z}, \qquad t = \frac{L}{U_0}\tilde{t}, \qquad \eta = h_1\tilde{\eta},$$

$$p_2 = (\rho_1 U_0^2)\tilde{p}_2, \qquad u_2 = \sqrt{\beta}U_0\tilde{u}_2, \qquad w_2 = \sqrt{\beta}U_0\tilde{w}_2.$$

This naturally suggests that we introduce the velocity potencial $\phi = \sqrt{\beta} U_0 L \tilde{\phi}$. Note that the definition for $\tilde{z}$ is different from the one for the upper region, since it involves the characteristic wavelength $L$ instead of the vertical scale $h_2$. This is consistent since both scales are of the same order.

In these dimensionless variables, the Bernoulli law for the interface reads

$$\sqrt{\beta}\,\phi_t + \frac{\beta}{2}(\phi_x^2 + \phi_z^2) + \eta + \frac{\rho_1}{\rho_2} P = C(t),$$

where the tilde has been ignored. $C(t)$ is an arbitrary function of time. Then, up to order $\beta$, the pressure derivative $P_x$ is

$$P_x = -\frac{\rho_2}{\rho_1}\left(\eta_x + \sqrt{\beta}\,\left(\phi_t(x, \sqrt{\beta}\eta, t)\right)_x\right) + O(\beta), \tag{2.19}$$

where $\phi$ satisfies the Neumann problem with a free upper surface boundary condition, given as

$$\begin{cases} \phi_{xx} + \phi_{zz} = 0, & \text{on } -\dfrac{h_2}{L} + \dfrac{h_2 h(Lx/l)}{L} \le z \le \sqrt{\beta}\,\eta(x,t), \\ \phi_z = \eta_t + \sqrt{\beta}\,\eta_x \phi_x, & \text{at } z = \sqrt{\beta}\,\eta(x,t), \\ -\dfrac{h_2}{l} h'(Lx/l)\phi_x + \phi_z = 0, & \text{at } z = -\dfrac{h_2}{L} + \dfrac{h_2 h(Lx/l)}{L}. \end{cases} \tag{2.20}$$

Furthermore,

$$\begin{aligned}\left[\sqrt{\beta}\phi_t\left(x,\sqrt{\beta}\eta,t\right)\right]_x &= \sqrt{\beta}\phi_{tx}\left(x,\sqrt{\beta}\eta,t\right)+\beta\phi_{tz}\left(x,\sqrt{\beta}\eta,t\right)\eta_x,\\ &= \sqrt{\beta}\phi_{tx}\left(x,\sqrt{\beta}\eta,t\right)+O(\beta),\\ &= \sqrt{\beta}\phi_{tx}(x,0,t)+O(\beta),\end{aligned}$$

where a Taylor expansion about $z = 0$ was performed.

Therefore,

$$P_x = -\frac{\rho_2}{\rho_1}\left(\eta_x + \sqrt{\beta}\,\phi_{tx}(x,0,t)\right)+O(\beta). \tag{2.21}$$

As in the flat bottom case [8], from Eq. (2.21) it is clear that it is sufficient to find the horizontal velocity $\phi_x$ at $z = 0$ in order to obtain $P_x$ at the interface. Due to the presence of the small parameter $\sqrt{\beta}$ in problem (2.20), $\phi_x(x,0,t)$ can be approximated by the horizontal velocity at $z = 0$ that comes from the linearized problem around $z = 0$,

$$\begin{cases}\phi_{xx}+\phi_{zz}=0, & \text{on } -\dfrac{h_2}{L}+\dfrac{h_2 h(Lx/l)}{L}\le z\le 0,\\[2ex] \phi_z=\eta_t, & \text{at } z=0,\\[2ex] -\dfrac{h_2}{l}h'(Lx/l)\phi_x+\phi_z=0, & \text{at } z=-\dfrac{h_2}{L}+\dfrac{h_2 h(Lx/l)}{L}.\end{cases} \tag{2.22}$$

In this systematic reduction we use Taylor expansion to ensure that

$$\begin{aligned}\phi_z(x,0,t) &= \phi_z\left(x,\sqrt{\beta}\,\eta,t\right)+O\left(\sqrt{\beta}\right),\\ &= \eta_t+\sqrt{\beta}\,\eta_x\phi_x+O\left(\sqrt{\beta}\right),\end{aligned}$$

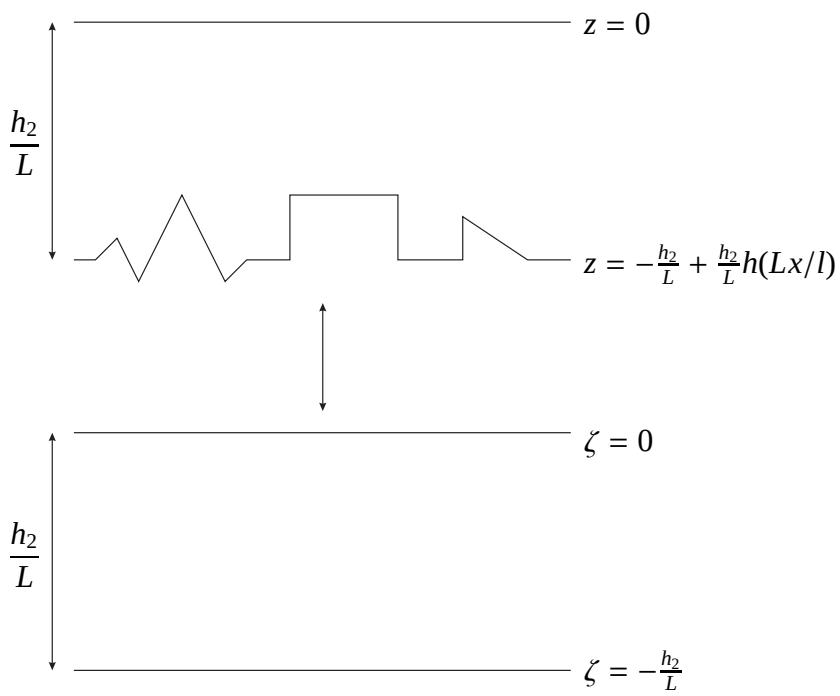


Figure 2.2: Conformal mapping, $(x, z) = (\mathrm{x}(\xi, \zeta), \mathrm{z}(\xi, \zeta))$.

and therefore,

$$\phi_z(x, 0, t) = \eta_t + O\left(\sqrt{\beta}\right).$$

To find the horizontal velocity $\phi_x(x, 0, t)$ in problem (2.22), a conformal mapping between the flat strip $\zeta \in \left[-\frac{h_2}{L}, 0\right]$ and the lower layer at rest is performed. See Fig. 2.2.

The problem in conformal coordinates is

$$\begin{cases} \phi_{\xi\xi} + \phi_{\zeta\zeta} = 0, & \text{on } -\dfrac{h_2}{L} \le \zeta \le 0, \\ \phi_\zeta(\xi, 0, t) = M(\xi)\, \eta_t(\mathrm{x}(\xi, 0), t), & \text{at } \zeta = 0, \\ \phi_\zeta = 0, & \text{at } \zeta = -\dfrac{h_2}{L}, \end{cases} \tag{2.23}$$

where the previous Neumann condition at the top is now modified by $M(\xi) = \mathrm{z}_\zeta(\xi, 0)$ which is the nonzero element of the Jacobian of the conformal mapping at the unperturbed interface. As shown in [24], its exact expression is:

$$M(\xi_0) = 1 - \frac{\pi}{4}\frac{L}{h_2}\int_{-\infty}^{\infty} \frac{h(L\mathrm{x}(\xi, -h_2/L)/l)}{\cosh^2\left(\frac{\pi L}{2h_2}(\xi - \xi_0)\right)}\, d\xi.$$

Moreover, the Jacobian along the unperturbed interface is an analytic function.

Hence a highly complex boundary profile has been converted into a smooth variable coefficient in the equations.

To obtain the Neumann condition at the unperturbed interface in problem (2.23), consider

$$\phi_\zeta = \phi_x \mathrm{x}_\zeta + \phi_z \mathrm{z}_\zeta$$

evaluated at $z = 0$ (equivalently $\zeta = 0$):

$$\phi_\zeta(\xi, 0, t) = \phi_x(x, 0, t)\, \mathrm{x}_\zeta(\xi, 0) + \phi_z(x, 0, t)\, \mathrm{z}_\zeta(\xi, 0).$$

The Cauchy-Riemann relations and the fact that $\mathrm{z}(\xi, 0) = 0$ and $\mathrm{z}_\xi(\xi, 0) = 0$ imply

that $\mathrm{x}_\zeta(\xi, 0) = 0$, which leads to the Neumann condition in problem (2.23).

Since a conformal mapping was used in the coordinate transformation and $\mathrm{z}_\xi(\xi, 0) = 0$, it is guaranteed that $\mathrm{z}_\zeta(\xi, 0) = \mathrm{x}_\xi(\xi, 0)$ is different from zero. From $\phi_\xi(\xi, 0, t) = \phi_x(x, 0, t)\,\mathrm{x}_\xi(\xi, 0)$, the velocity $\phi_x(x, 0, t)$ is recovered as

$$\phi_x(x, 0, t) = \frac{\phi_\xi(\xi, 0, t)}{M(\xi)}.$$

The bottom Neumann condition is trivial in these new coordinates.

Notice that the terrain-following velocity component $\phi_\xi(\xi, 0, t)$ is a tangential derivative on the boundary for problem (2.23). Hence it can be obtained as the Hilbert transform on the strip (see [15]) applied to the Neumann data. Namely

$$\phi_\xi(\xi, 0, t) = \mathcal{T}\left[\phi_\zeta(\tilde{\xi}, 0, t)\right](\xi),$$

and substituting the Neumann data from problem (2.23),

$$\phi_\xi(\xi, 0, t) = \mathcal{T}\left[M(\tilde{\xi})\eta_t(\mathrm{x}(\tilde{\xi}, 0), t)\right](\xi),$$

where

$$\mathcal{T}[f](\xi) = \frac{1}{2h} \fint f(\tilde{\xi}) \coth\left(\frac{\pi}{2h}(\tilde{\xi} - \xi)\right) d\tilde{\xi} \tag{2.24}$$

is the Hilbert transform on the strip of height $h$. In this case, $h = h_2/L$. The singular integral must be interpreted as a Cauchy principal value. The effect of the two-dimensional undisturbed layer below the interface is being collapsed onto a one-dimensional singular integral without any approximation. The results above are used in (2.21) by noting that $\phi_{tx}$ is obtained after taking the time derivative of

problem (2.22). Therefore,

$$P_x = -\frac{\rho_2}{\rho_1}\left(\eta_x + \sqrt{\beta}\,\frac{1}{M(\xi)}\mathcal{T}\left[M(\tilde{\xi})\eta_{tt}(\mathrm{x}(\tilde{\xi},0),t)\right](\xi)\right) + O(\beta). \tag{2.25}$$

Now, $\phi_x(x,0,t)$ is a tangential derivative on the flat upper boundary for problem (2.22), whose domain is a corrugated strip. Hence, it is also expressed as a Hilbert transform acting on Neumann data. Since

$$\phi_x(x,0,t) = \frac{L}{2h_2 M(\xi(x,0))}\fint M(\tilde{\xi})\,\eta_t(\mathrm{x}(\tilde{\xi},0),t)\coth\left(\frac{\pi L}{2h_2}(\tilde{\xi}-\xi(x,0))\right)\,d\tilde{\xi},$$

a Hilbert-like transform on the corrugated strip has been identified as:

$$\mathcal{T}_c[f](x) = \frac{L}{2h_2 M(\xi(x,0))}\fint M(\tilde{\xi})\,f(\mathrm{x}(\tilde{\xi},0))\coth\left(\frac{\pi L}{2h_2}(\tilde{\xi}-\xi(x,0))\right)\,d\tilde{\xi},$$

which is not a convolution operator, unlike Eq. (2.24).

Finally, substituting the expression for $P_x$ obtained in Eq. (2.25) in the upper layer averaged equations (2.18) gives

$$\begin{cases} \eta_t - [(1-\eta)\overline{u_1}]_x = 0, \\ \overline{u_1}_t + \overline{u_1}\,\overline{u_1}_x + \left(1-\dfrac{\rho_2}{\rho_1}\right)\eta_x = \\ \qquad \sqrt{\beta}\dfrac{L}{2h_2}\dfrac{\rho_2}{\rho_1}\dfrac{1}{M(\xi(x,0))}\fint M(\tilde{\xi})\eta_{tt}(\mathrm{x}(\tilde{\xi},0),t)\coth\left(\dfrac{\pi L}{2h_2}(\tilde{\xi}-\xi(x,0))\right)\,d\tilde{\xi} + O(\beta). \end{cases}$$

In a compact notation this becomes

$$\begin{cases} \eta_t - [(1-\eta)\overline{u_1}]_x = 0, \\ \overline{u_1}_t + \overline{u_1}\,\overline{u_1}_x + \left(1-\dfrac{\rho_2}{\rho_1}\right)\eta_x = \sqrt{\beta}\dfrac{\rho_2}{\rho_1}\dfrac{1}{M(\xi)}\mathcal{T}\left[M(\cdot)\eta_{tt}(\mathrm{x}(\cdot,0),t)\right](\xi) + O(\beta), \end{cases}$$

where the dot indicates the variable on which the operator $\mathcal{T}$ is applied.

It remains to make a few manipulations with this set of equations: eliminate the second order derivative in time and write all spatial derivatives in the $\xi$-variable.

Note that the first equation is exact. According to it $\eta_{tt} = ((1-\eta)\overline{u_1})_{xt}$ so only the first time derivative of $\overline{u_1}$ needs to enter the right-hand side of the second equation.

In conclusion, the reduced one-dimensional internal wave model is:

$$\begin{cases} \eta_t - [(1-\eta)\overline{u_1}]_x = 0, \\ \overline{u_1}_t + \overline{u_1}\,\overline{u_1}_x + \left(1 - \dfrac{\rho_2}{\rho_1}\right)\eta_x = \sqrt{\beta}\dfrac{\rho_2}{\rho_1}\dfrac{1}{M(\xi)}\mathcal{T}\left[M(\cdot)((1-\eta)\overline{u_1})_{xt}(\mathrm{x}(\cdot,0),t)\right]. \end{cases} \tag{2.26}$$

The transform in the forcing term is in curvilinear coordinates. For practical purposes both sides must be in the same coordinate system, which is readily adjusted via the conformal mapping: every $x$-derivative is equal to a $\xi$-derivative divided by the Jacobian $M(\xi)$. Therefore, system (2.26) in the terrain-following coordinates reads

$$\begin{cases} \eta_t - \dfrac{1}{M(\xi)}[(1-\eta)\overline{u_1}]_\xi = 0, \\ \overline{u_1}_t + \dfrac{1}{M(\xi)}\overline{u_1}\,\overline{u_1}_\xi + \dfrac{1}{M(\xi)}\left(1 - \dfrac{\rho_2}{\rho_1}\right)\eta_\xi = \sqrt{\beta}\dfrac{\rho_2}{\rho_1}\dfrac{1}{M(\xi)}\mathcal{T}\left[((1-\eta)\overline{u_1})_{\xi t}\right]. \end{cases} \tag{2.27}$$

This is a Boussinesq-type system with variable (time independent) coefficients depending on $M(\xi)$ for the perturbation of the interface $\eta$ and the mean-layer horizontal upper velocity $\overline{u_1}$. We will show that this is a dispersive model, where the dispersion term comes in through the Hilbert transform. Since no smallness

assumption was made on the wave amplitude up to now, the model derived is strongly nonlinear. It involves a Hilbert transform on the strip characterizing the presence of harmonic functions (hence the potential flow) below the interface.

System (2.27) is a reduction of the original Euler equations constituted by a pair of 2D-systems of PDEs to a single 1D-system of PDEs at the interface. Instead of the integration of the Euler equations in the presence of a free interface, a single 1D-system of PDEs is to be solved. Efficient computational methods can be produced for this accurate reduced model which governs, to leading order, a complex two-dimensional problem.

Remarks:

1. If the bottom is flat, $M(\xi) = 1$ and the same system derived in [8] is recovered, which is a nice consistency check.

2. When the lower depth tends to infinity ($h_2 \to \infty$) the limit for this model is the same one obtained in [8] because the bottom is not seen anymore ($M(\xi) \to 1$ and $\mathrm{x}(\tilde{\xi}, 0) \to \tilde{\xi}$). Therefore

$$\phi_{xt}(x, 0, t) \to \frac{1}{\pi} \fint \frac{((1-\eta)\overline{u_1})_{xt}(\tilde{x}, t)}{\tilde{x} - x}\, d\tilde{x} = \mathcal{H}\Big[((1-\eta)\overline{u_1})_{xt}\Big](x),$$

   where $\mathcal{H}$ is the usual Hilbert transform defined as

$$\mathcal{H}[f](x) = \frac{1}{\pi} \fint \frac{f(\tilde{x})}{\tilde{x} - x}\, d\tilde{x}.$$

   In this (shallow upper layer) infinite lower layer regime, system (2.26) be-

comes

$$\begin{cases} \eta_t - [(1-\eta)\overline{u_1}]_x = 0, \\ \overline{u_1}_t + \overline{u_1}\,\overline{u_1}_x + \left(1 - \dfrac{\rho_2}{\rho_1}\right)\eta_x = \sqrt{\beta}\dfrac{\rho_2}{\rho_1}\mathcal{H}\left[((1-\eta)\overline{u_1})_{xt}\right]. \end{cases} \tag{2.28}$$

3. The Fourier Transform (FT) of a Hilbert transform is easily computed. We now make a comment regarding the use of FTs in numerical schemes. The operators $\mathcal{T}[f]$ and $\mathcal{H}[f]$ have Fourier transforms

$$\widehat{\mathcal{T}[f]} = i\coth\left(\frac{kh_2}{L}\right)\hat{f},$$
$$\widehat{\mathcal{H}[f]} = i\,\mathrm{sgn}(k)\,\hat{f},$$

where the operator symbol multiplies the transform of $f$, which is $\hat{f}$. Therefore in Eqs. (2.27) and (2.28) a pseudospectral scheme would apply a DFT to the terms inside the square brackets. FFTs are only aplicable directly when $M(\xi) = 1$ and the waves are weakly nonlinear.

## 2.3 Dispersion relation for the linearized model

Consider the flat bottom case in system (2.26), that is, $M \equiv 1$:

$$\begin{cases} \eta_t - [(1-\eta)\overline{u_1}]_x = 0, \\ \overline{u_1}_t + \overline{u_1}\,\overline{u_1}_x + \left(1 - \dfrac{\rho_2}{\rho_1}\right)\eta_x = \dfrac{\rho_2}{\rho_1}\sqrt{\beta}\,\mathcal{T}\left[((1-\eta)\overline{u_1})_{xt}\right] + O(\beta). \end{cases}$$

Its linearization around the undisturbed state $\eta = 0$, $\overline{u_1} = 0$ gives:

$$\begin{cases} \eta_t - \overline{u_1}_x = 0, \\ \overline{u_1}_t + \left(1 - \dfrac{\rho_2}{\rho_1}\right)\eta_x = \dfrac{\rho_2}{\rho_1}\sqrt{\beta}\,\mathcal{T}\left[\overline{u_1}_{xt}\right]. \end{cases}$$

By differentiating once in $t$, $\eta$ can be eliminated from the second equation:

$$\overline{u_1}_{tt} + \left(1 - \frac{\rho_2}{\rho_1}\right)\overline{u_1}_{xx} = \frac{\rho_2}{\rho_1}\sqrt{\beta}\,\mathcal{T}\left[\overline{u_1}_{xtt}\right].$$

Let $\overline{u_1} = Ae^{i(kx-\omega t)}$ and substituting above,

$$e^{i(kx-\omega t)}\left(-\omega^2 - \left(1 - \frac{\rho_2}{\rho_1}\right)k^2\right) = \frac{\rho_2}{\rho_1}\sqrt{\beta}\,k\omega^2\,e^{-i\omega t}\,\mathcal{T}\left[-ie^{ikx}\right].$$

Since $\mathcal{T}[e^{ikx}] = i\coth\left(\frac{kh_2}{L}\right)e^{ikx}$,

$$\omega^2 = \frac{\left(\frac{\rho_2}{\rho_1} - 1\right)k^2}{1 + \frac{\rho_2}{\rho_1}\sqrt{\beta}k\coth\left(\frac{kh_2}{L}\right)}, \tag{2.29}$$

which is the correct approximation for the full dispersion relation

$$\omega^2 = \frac{\left(\frac{\rho_2}{\rho_1} - 1\right)k^2}{\frac{kh_1}{L}\coth\left(\frac{kh_1}{L}\right) + \frac{\rho_2}{\rho_1}\sqrt{\beta}k\coth\left(\frac{kh_2}{L}\right)}$$

when $kh_1$ is near zero. A nonvanishing value of the parameter $\beta$ in the dispersion relation makes the phase velocity a function of the wave number $k$. Observe that $\frac{\omega^2}{k^2} \to 0$ as $k \to \infty$, so bounded phase velocities are obtained as $k$ becomes large. This is a good property for numerical schemes.

In the limit $h_2 \to \infty$ the operator $\mathcal{T}$ becomes $\mathcal{H}$. Since $\mathcal{H}[e^{ikx}] = i\,\mathrm{sgn}(k)e^{ikx}$,

the dispersion relation for system (2.28) is

$$\omega^2 = \frac{\left(\frac{\rho_2}{\rho_1} - 1\right) k^2}{1 + \frac{\rho_2}{\rho_1}\sqrt{\beta}\,|k|}$$

and $\frac{\omega^2}{k^2} \to 0$ as $k \to \infty$.

## 2.4 Unidirectional wave regime

For weakly nonlinear unidirectional waves and slowly varying topography, our model reduces to a single ILW equation with variable coefficients.

Consider again system (2.26), except for the Jacobian of the conformal mapping which now is

$$M(\xi_0) = 1 - \frac{\pi}{4}\frac{L}{h_2}\int_{-\infty}^{\infty} \frac{h(\varepsilon \mathrm{x}(\xi, -h_2/L))}{\cosh^2\left(\frac{\pi L}{2h_2}(\xi - \xi_0)\right)}\, d\xi,$$

since we assume a slowly varying bottom topography described in non-dimensional coordinates as $z = -\frac{h_2}{L} + \frac{h_2}{L}h(\varepsilon x)$, with $\varepsilon \ll 1$. The restriction to a slowly varying topography is consistent with the objective of the present Section, which is to find equations to model the unidirectional wave propagation. Hence there will be no reflection nor any backward evolution opposite to the propagation direction.

To study the weakly nonlinear regime, we introduce the typical amplitude $a$ for the perturbation of the interface and introduce the nonlinearity parameter $\alpha = \frac{a}{h_1}$ of order $O\left(\sqrt{\beta}\right)$. As usual in a weakly nonlinear theory we set $\eta = \alpha\eta^*$. With this, the original dimensional perturbation $\eta$ is non-dimensionalized as $\eta = \alpha h_1 \eta^* = a\eta^*$. We also state that $\overline{u_1} = \alpha c_0 \overline{u_1}^*$, $t = \frac{t^*}{c_0}$ where $c_0^2 = \left(\frac{\rho_2}{\rho_1} - 1\right)$. Depending on the root

$c_0$ chosen, there will be a right- or left-travelling wave.

Then, dropping the asterisks, Eq. (2.26) becomes

$$\begin{cases} \eta_t - [(1-\alpha\eta)\overline{u_1}]_x = 0, \\ \overline{u_1}_t + \alpha\overline{u_1}\,\overline{u_1}_x - \eta_x = \sqrt{\beta}\dfrac{\rho_2}{\rho_1}\dfrac{1}{M(\xi)}\mathcal{T}\left[M(\tilde{\xi})[(1-\alpha\eta)\overline{u_1}]_{xt}\right] + O(\beta). \end{cases} \tag{2.30}$$

Note that

$$\eta_t = \overline{u_1}_x + O(\alpha); \qquad \eta_x = \overline{u_1}_t + O\left(\alpha, \sqrt{\beta}\right). \tag{2.31}$$

As in [8], we look for a solution, up to a first order correction in $\alpha$ and $\sqrt{\beta}$, in the form

$$\eta = A_1\overline{u_1} + \alpha A_2\overline{u_1}^2 + \sqrt{\beta}A_3\frac{1}{M(\xi)}\mathcal{T}\left[M(\tilde{\xi})\overline{u_1}_t\right]. \tag{2.32}$$

Substituting in the system of Eqs. (2.30) up to order $\alpha$, $\sqrt{\beta}$, two equations for $\overline{u_1}$ are obtained:

$$0 = A_1\overline{u_1}_t + 2\alpha A_2\overline{u_1}\,\overline{u_1}_t + 2\alpha A_1\overline{u_1}\,\overline{u_1}_x - \overline{u_1}_x + \sqrt{\beta}A_3\frac{1}{M(\xi)}\mathcal{T}\left[M(\tilde{\xi})\overline{u_1}_{tt}\right]$$

and

$$0 = \overline{u_1}_t + \alpha\overline{u_1}\,\overline{u_1}_x - \left[A_1\overline{u_1}_x + 2\alpha A_2\overline{u_1}\,\overline{u_1}_x + \sqrt{\beta}A_3\frac{1}{M(\xi)}\mathcal{T}\left[M(\tilde{\xi})\overline{u_1}_{xt}\right]\right] - \\ - \sqrt{\beta}\frac{\rho_2}{\rho_1}\frac{1}{M(\xi)}\mathcal{T}\left[M(\tilde{\xi})\overline{u_1}_{xt}\right] + O\left(\alpha^2, \beta, \alpha\sqrt{\beta}\right).$$

For compatibility $A_1 = \pm 1$ and to choose a right-going wave we take $A_1 = -1$. Therefore

$$\eta_x = -\overline{u_1}_x + O\left(\alpha, \sqrt{\beta}\right), \tag{2.33}$$

so $\overline{u_1}_t = -\overline{u_1}_x + O\left(\alpha,\ \sqrt{\beta}\right)$ and $\overline{u_1}_{tt} = -\overline{u_1}_{xt} + O\left(\alpha,\ \sqrt{\beta}\right)$ and the two equations are consistent if $A_1 = -1$, $A_2 = -\frac{1}{4}$ and $A_3 = -\frac{\rho_2}{2\rho_1}$. As a result, the evolution equation for $\overline{u_1}$ is

$$\overline{u_1}_t + \frac{3}{2}\alpha\overline{u_1}\,\overline{u_1}_x + \overline{u_1}_x - \frac{\rho_2}{\rho_1}\frac{\sqrt{\beta}}{2}\frac{1}{M(\xi)}\mathcal{T}\left[M(\tilde{\xi})\overline{u_1}_{xt}\right] = O\left(\beta, \alpha^2, \alpha\sqrt{\beta}\right).$$

For the elevation of the interface $\eta$ a similar equation can be obtained through asymptotic relations which permit (to leading order) to exchange derivatives in $\eta$ by derivatives in $\overline{u_1}$, as well as time derivatives for spatial derivatives. This is a consequence of (2.32). To begin with, use that

$$\overline{u_1}_{xt} = -\eta_{xt} + O\left(\alpha,\ \sqrt{\beta}\right)$$

so

$$\frac{\sqrt{\beta}}{2}\frac{\rho_2}{\rho_1}\frac{1}{M(\xi)}\mathcal{T}\left[M(\tilde{\xi})\overline{u_1}_{xt}\right] = -\frac{\sqrt{\beta}}{2}\frac{\rho_2}{\rho_1}\frac{1}{M(\xi)}\mathcal{T}\left[M(\tilde{\xi})\eta_{xt}\right] + O\left(\alpha^2, \beta, \alpha\sqrt{\beta}\right). \quad (2.34)$$

In virtue of Eqs. (2.33) and (2.32)

$$\begin{aligned}\frac{3}{2}\alpha\overline{u_1}\,\overline{u_1}_x &= \frac{3}{2}\alpha\left(-\eta_x + O\left(\alpha,\ \sqrt{\beta}\right)\right)\left(-\eta + O\left(\alpha,\ \sqrt{\beta}\right)\right), \\ &= \frac{3}{2}\alpha\eta\eta_x + O\left(\alpha^2, \alpha\sqrt{\beta}\right), \end{aligned} \quad (2.35)$$

and for similar reasons

$$\eta_t + \eta_x = -(\overline{u_1}_t + \overline{u_1}_x) - \frac{\alpha}{2}\overline{u_1}(\overline{u_1}_t + \overline{u_1}_x) - \frac{\sqrt{\beta}}{2}\frac{\rho_2}{\rho_1}\frac{1}{M(\xi)}\mathcal{T}\left[M(\tilde{\xi})(\overline{u_1}_{tt} + \overline{u_1}_{xt})\right],$$
$$= -(\overline{u_1}_t + \overline{u_1}_x) + O\left(\alpha^2, \alpha\sqrt{\beta}, \beta\right). \tag{2.36}$$

Substituting all these expressions in the evolution equation for $\overline{u_1}$ we obtain the evolution equation for the elevation of the interface,

$$\eta_t + \eta_x - \frac{3}{2}\alpha\eta\eta_x - \frac{\rho_2}{\rho_1}\frac{\sqrt{\beta}}{2}\frac{1}{M(\xi)}\mathcal{T}\left[M(\tilde{\xi})\eta_{xt}\right] = O\left(\beta, \alpha^2, \alpha\sqrt{\beta}\right).$$

Finally, in curvilinear coordinates we have

$$\eta_t + \frac{1}{M(\xi)}\eta_\xi - \frac{3}{2}\frac{\alpha}{M(\xi)}\eta\eta_\xi - \frac{\rho_2}{\rho_1}\frac{\sqrt{\beta}}{2}\frac{1}{M(\xi)}\mathcal{T}[\eta_{\xi t}] = 0. \tag{2.37}$$

This is an ILW equation with variable coefficients accounting for the slowly varying bottom topography. Instead of the usual Hilbert transform on the half-space, a Hilbert transform on the strip appears. The dispersion relation for the flat bottom case ($M(\xi) = 1$) is

$$\omega = \frac{k}{1 + \frac{\rho_2}{\rho_1}\frac{\sqrt{\beta}}{2}k\coth\left(\frac{kh_2}{L}\right)}. \tag{2.38}$$

The equation reduces to a regularized dispersive model in analogy with the Benjamin-Bona-Mahony equation (BBM), [4].

Remarks:

1. The constant coefficient version of Eq. (2.37) differs from the ILW consid-

ered in [8], Eq. (4.33), page 23, in that the latter has a dispersion term with spatial derivatives only, as in the KdV equation. Both constant coefficient equations are equivalent up to the order considered since we can substitute $\eta_{\xi t}$ by $-\eta_{\xi\xi}$ in the dispersion term up to order $O\left(\beta, \alpha\sqrt{\beta}\right)$. There are two advantages for our choice. First, for every change from a Cartesian $x$-derivative to a curvilinear $\xi$-derivative we need the presence of the metric term $M(\xi)$. Hence for the Camassa-Choi model with the second order $x$-derivative we would end up with a variable coefficient within the nonlocal operator. Second, the regularized dispersive operator (namely with an $xt$-derivative) leads to the stable dispersion relation (2.38) regarding numerical schemes. Short waves have bounded propagation speeds. This does not happen with the ILW equation considered in [8], whose dispersion relation is

$$\omega = k - \frac{\rho_2}{\rho_1}\frac{\sqrt{\beta}}{2}k^2 \coth\left(\frac{kh_2}{L}\right).$$

2. One step remains to be explained in the substitution of Eq. (2.32) into the second equation of system (2.30), namely why it is valid (for slowly varying topography) that

$$\left(\frac{\sqrt{\beta}}{M(\xi)}\mathcal{T}\left[M(\tilde{\xi})\overline{u_1}_t\right]\right)_x = \frac{\sqrt{\beta}}{M(\xi)}\mathcal{T}\left[M(\tilde{\xi})\overline{u_1}_{tx}\right] + O(\beta). \tag{2.39}$$

This approximation was not presented in [8] since the present work contains for the first time the conformal mapping technique used for the lower layer. The approximation (2.39) is justified through the construction of an auxiliary PDE problem. See Appendix A for details.

3. For system (2.28) a similar unidirectional reduction can be obtained leading to

$$\eta_t + \eta_x - \frac{3}{2}\alpha\eta\eta_x - \frac{\rho_2}{\rho_1}\frac{\sqrt{\beta}}{2}\mathcal{H}[\eta_{xt}] = 0,$$

which is a regularized Benjamin-Ono (BO) equation over an infinite bottom layer.

Hence Eq. (2.37) is a generalization of the BO equation for intermediate depth and the presence of a topography. This equation is valid only when backscattering is negligible.

## 2.5 Solitary wave solutions

The ILW equation we referred to in Section 2.4 and derived in [8, 14, 17] is of the form

$$\eta_t + \eta_\xi + c_1\eta\eta_\xi + c_2\mathcal{T}[\eta_{\xi\xi}] = 0 \tag{2.40}$$

where $c_1 = -\frac{3}{2}\alpha$ and $c_2 = \frac{\rho_2}{\rho_1}\frac{\sqrt{\beta}}{2}$. Eq. (2.40) admits a family in the parameter $\theta$ of solitary wave solutions [14, 8]

$$\eta(x) = \frac{a\cos^2\theta}{\cos^2\theta + \sinh^2(x/\lambda)}, \quad x = \xi - ct, \tag{2.41}$$

where

$$a = \frac{4c_2\theta\tan\theta}{h_2c_1}, \quad \lambda = \frac{h_2}{\theta}, \quad c = 1 - \frac{2c_2}{h_2}\theta\cot(2\theta),$$

with $0 \le \theta \le \pi/2$. Alternatively, we consider a Regularized Intermediate Long Wave equation

$$\eta_t + \eta_\xi + c_1\eta\eta_\xi - c_2\mathcal{T}[\eta_{\xi t}] = 0 \tag{2.42}$$

to the same order of approximation. It also admits the solitary wave solution Eq. (2.41) with

$$a = \frac{4c_2}{h_2 c_1} \frac{\theta \tan\theta}{1 + \frac{2c_2}{h_2}\theta \cot(2\theta)}, \quad \lambda = \frac{h_2}{\theta}, \quad c = \frac{1}{1 + \frac{2c_2}{h_2}\theta \cot(2\theta)}.$$

In the numerical section we will present a few experiments with solitary waves over a flat bottom. In the near future we intend to study solitary waves interacting with highly varying topography and submarine structures.

# Chapter 3

# A higher-order reduced model

Since we want to study wave interaction with highly variable topographies and submarine structures, we need to be able to account for higher order (vertical) coupling terms between the two layers. Namely we want to investigate if these higher order terms do indeed play a role in the dynamics. Hence in this chapter we improve the model from the previous chapter regarding the pressure term by allowing nonhydrostatic terms to come into play.

## 3.1 Higher-order upper layer equations

The purpose of this chapter is to improve the order of approximation of system (2.27) by using higher precision approximations for the pressure term with respect to the dispersion parameter $\beta$. Instead of order $\beta$, we seek order $O(\beta^{3/2})$. We start with the mean-layer equations (2.10) and (2.17) obtained in Section 2.1.

For convenience they are repeated here:

$$\eta_{1t} + (\eta_1 \overline{u_1})_x = 0, \tag{3.1}$$

$$\overline{u_1}_t + \overline{u_1} \cdot \overline{u_1}_x = -\overline{p_1}_x + O(\beta^2). \tag{3.2}$$

To approximate $\overline{p_1}_x$ with order $\beta^{3/2}$ we need to expand $p_1(x, z, t)$ with one more term:

$$p_1(x, z, t) = p_1^{(0)} + \beta p_1^{(1)} + O(\beta^2),$$

so its vertical derivative is expanded as

$$p_{1z}(x, z, t) = p_1^{(0)}{}_z + \beta p_1^{(1)}{}_z + O(\beta^2). \tag{3.3}$$

Again, from the vertical momentum equation

$$p_{1z} = -1 - \beta(w_{1t} + u_1 w_{1x} + w_1 w_{1z})$$

we have that

$$p_1^{(0)}{}_z = -1.$$

This is the hydrostatic contribution to the pressure. We also have that

$$p_1^{(1)}{}_z = -(w_1^{(0)}{}_t + u_1^{(0)} w_1^{(0)}{}_x + w_1^{(0)} w_1^{(0)}{}_z).$$

Even though the upper layer is shallow, through $p_1$ we can compute the leading order nonhydrostatic correction.

Let $D_1 = \partial t + u_1^{(0)} \partial x$ be the leading order material derivative. We rewrite the

expression above as

$$p_{1\ z}^{(1)} = -D_1 w_1^{(0)} - w_{1\ z}^{(0)} w_1^{(0)}. \tag{3.4}$$

Let us express the quantities $w_{1\ z}^{(0)}$ and $w_1^{(0)}$ in terms of $\eta$ and $\overline{u_1}$. We begin by expanding the incompressibility equation to obtain

$$w_{1\ z}^{(0)} = -u_{1\ x}^{(0)}(x,t). \tag{3.5}$$

Integrating Eq. (3.5) from $\eta$ to $z \leq 1$ and taking into account the $z$-independence expressed by Eq. (2.12) we have that

$$w_1^{(0)}(x,z,t) = -u_{1\ x}^{(0)}(x,t)(z-\eta) + w_1^{(0)}\Big|_{z=\eta(x,t)}.$$

Now, from the kinematic condition in Eq. (2.2), to leading order

$$w_1^{(0)}\Big|_{z=\eta(x,t)} = \eta_t + u_1^{(0)}\eta_x$$

so

$$w_1^{(0)}(x,z,t) = -u_{1\ x}^{(0)}(x,t)(z-\eta) + \eta_t + u_1^{(0)}\eta_x,$$

that is,

$$w_1^{(0)}(x,z,t) = -u_{1\ x}^{(0)}(x,t)(z-\eta) + D_1\eta. \tag{3.6}$$

Substituting Eqs. (3.6) and (3.5) in Eq. (3.4):

$$p_{1\ z}^{(1)} = (z-\eta)\left(D_1(u_{1\ x}^{(0)}) - u_{1\ x}^{(0)2}\right) - D_1^2(\eta).$$

Since

$$\overline{u_1} = u_1^{(0)} + O(\beta), \tag{3.7}$$

it is also valid that

$$p_{1\ z}^{(1)} = (z-\eta)\left(D_1(\overline{u_1}_x) - \overline{u_1}_x^2\right) - D_1^2(\eta) + O(\beta).$$

Recall that $\eta_1 = 1 - \eta$ and now define

$$G_1(x,t) = \frac{1}{\eta_1}(D_1^2\eta).$$

It can be shown[1] that

$$G_1(x,t) = D_1(\overline{u_1}_x) - \overline{u_1}_x^2 + O(\beta).$$

Therefore,

$$p_{1\ z}^{(1)} = (z-\eta)G_1(x,t) - \eta_1 G_1(x,t) + O(\beta)$$

[1]Write the conservation of mass Eq. (2.10) in the form

$$(\partial t + \overline{u_1}\partial x)\eta_1 + \eta_1\overline{u_1}_x = 0,$$

which together with the approximation (3.7) leads to

$$D_1\eta_1 + \eta_1\overline{u_1}_x = O(\beta),$$

which is the same as $D_1\eta = \eta_1\overline{u_1}_x + O(\beta)$. Apply $D_1$ to it,

$$D_1^2\eta = D_1(\eta_1\overline{u_1}_x) + O(\beta).$$

Expanding the right-hand side above we have

$$\begin{aligned} D_1(\eta_1\overline{u_1}_x) + O(\beta) &= \eta_1(\overline{u_1}_{xt} + \overline{u_1}\,\overline{u_1}_{xx}) + \overline{u_1}_x(\eta_{1t} + \overline{u_1}\eta_{1x}) + O(\beta), \\ &= \eta_1(\overline{u_1}_{xt} + \overline{u_1}\,\overline{u_1}_{xx} - \overline{u_1}_x\,\overline{u_1}_x) + O(\beta), \\ &= \eta_1\left(D_1(\overline{u_1}_x) - \overline{u_1}_x^2\right) + O(\beta). \end{aligned}$$

Then $D_1^2\eta = \eta_1\left(D_1(\overline{u_1}_x) - \overline{u_1}_x^2\right) + O(\beta)$ as desired.

and substituting in the asymptotic expansion Eq. (3.3) for $p_{1z}$ we have

$$p_{1_z}(x,z,t) = -1 + \beta(z-1)G_1(x,t) + O(\beta^2).$$

Integrating from $z = \eta(x,t)$ to $z \leq 1$ we obtain

$$p_1(x,z,t) = P(x,t) - (z-\eta) + \beta G_1(x,t)\left(\frac{(z-1)^2}{2} - \frac{(\eta-1)^2}{2}\right) + O(\beta^2).$$

Differentiating once in $x$,

$$p_{1_x} = \eta_x + P_x(x,t) + \beta\left(G_1(x,t)\left(\frac{(z-1)^2}{2} - \frac{(\eta-1)^2}{2}\right)\right)_x + O(\beta^2)$$

and taking means

$$\overline{p_{1_x}} = \eta_x + P_x(x,t) - \frac{\beta}{\eta_1}\left(\frac{1}{3}\eta_1^3 G_1(x,t)\right)_x + O(\beta^2).$$

Substituting in Eq. (3.2) we have

$$\overline{u_{1_t}} + \overline{u_1}\cdot\overline{u_{1_x}} = -\left(\eta_x + P_x(x,t) - \frac{\beta}{\eta_1}\left(\frac{1}{3}\eta_1^3 G_1(x,t)\right)_x\right) + O(\beta^2). \qquad (3.8)$$

If the lower fluid layer is neglected and $P$ is regarded as the external pressure applied to the free surface, Eqs. (3.1) and (3.8) are the complete set of evolution equations for one homogeneous layer derived by Su and Gardner in [27] and independently by Green and Naghdi in [11].

## 3.2 Improved approximation for pressure at the interface

Now we want an approximation of order $O(\beta^{\frac{3}{2}})$ for $P_x(x,t) = \Big(p_2(x,\eta(x,t),t)\Big)_x$ from the Euler equations for the lower fluid layer. This order of approximation is sufficient to make the nonhydrostatic order $\beta$ terms explicit in the asymptotic expansion. Again, the scale $\sqrt{\beta}$ comes from the lower layer reduction.

From the Bernoulli law for the lower layer:

$$P(x,t) = -\frac{\rho_2}{\rho_1}\left(\sqrt{\beta}\phi_t + \frac{\beta}{2}(\phi_x^2 + \phi_z^2) + \eta + C(t)\right)\Big|_{z=\sqrt{\beta}\eta(x,t)}.$$

Using a Taylor expansion about $z = 0$ we obtain that

$$P(x,t) = -\frac{\rho_2}{\rho_1}\left(\eta + \sqrt{\beta}\left(\phi_t|_{z=0} + \sqrt{\beta}\eta\,\phi_{tz}|_{z=0}\right) + \frac{\beta}{2}\left(\phi_x^2\big|_{z=0} + \phi_z^2\big|_{z=0}\right) + C(t)\right) + O(\beta^{\frac{3}{2}}).$$

Since from Eq. (2.20) we have that $\phi_z = \eta_t + \sqrt{\beta}\eta_x\phi_x = \eta_t + O\left(\sqrt{\beta}\right)$ at $z = \sqrt{\beta}\eta(x,t)$, it follows that

$$\phi_z|_{z=0} = \phi_z|_{z=\sqrt{\beta}\eta} + O\left(\sqrt{\beta}\right) = \eta_t + O\left(\sqrt{\beta}\right)$$

and

$$\phi_{tz}|_{z=0} = \phi_{tz}|_{z=\sqrt{\beta}\eta} + O\left(\sqrt{\beta}\right) = \eta_{tt} + O\left(\sqrt{\beta}\right).$$

Therefore

$$P(x,t) = -\frac{\rho_2}{\rho_1}\left(\eta + \sqrt{\beta}\,\phi_t|_{z=0} + \beta\eta\eta_{tt} + \frac{\beta}{2}\left(\phi_x^2\big|_{z=0} + \eta_t^2\right) + C(t)\right) + O(\beta^{\frac{3}{2}})$$

and it is easy to take $x$-derivatives since all quantities are evaluated at $z = 0$:

$$P_x(x,t) = -\frac{\rho_2}{\rho_1}\left(\eta_x + \sqrt{\beta}\,\phi_{tx}|_{z=0} + \beta\left(\eta\eta_{tt} + \frac{1}{2}\eta_t^2 + \frac{1}{2}\,\phi_x^2\Big|_{z=0}\right)_x\right) + O(\beta^{\frac{3}{2}}).$$

Note from the previous chapter that $\phi_x|_{z=0}$ is already known up to order $\sqrt{\beta}$, namely that

$$\phi_x(\mathrm{x}(\xi,0),0,t) = \frac{1}{M(\xi)}\mathcal{T}\Big[M(\tilde{\xi})\eta_t(\mathrm{x}(\tilde{\xi},0),t)\Big](\xi) + O\left(\sqrt{\beta}\right) \tag{3.9}$$

which is all we need to approximate $\frac{1}{2}\,\phi_x^2\Big|_{z=0}$.

We will obtain $\phi_x|_{z=0}$ with order of approximation $\beta$ via the Hilbert transform on the corrugated strip. Assuming that our potential problem for the lower deep layer is defined in a region surrounding the physical domain containing the interface at rest $z = 0$, we restrict our potential problem to the unperturbed region. There the potential problem satisfies a certain upper Neumann boundary condition ($\phi_z|_{z=0}$) to be determined up to order $\beta$. This order of approximation is sufficient to obtain an $x$-derivative of order $\beta$ because we are solving a linear problem and we have the Hilbert transform connecting these two derivatives. The calculation is as follows.

To obtain $\phi_z|_{z=0}$ a Taylor expansion is used as before:

$$\phi_z\left(x,\sqrt{\beta}\eta\right) = \phi_z(x,0) + \sqrt{\beta}\eta\phi_{zz}(x,0) + O(\beta).$$

Since the boundary condition $\phi_z\left(x,\sqrt{\beta}\eta\right)$ is known we have

$$\phi_z(x,0) = \eta_t + \sqrt{\beta}\eta_x\phi_x(x,0) - \sqrt{\beta}\eta\phi_{zz}(x,0) + O(\beta)$$

and due to the Laplace equation,

$$\phi_z(x,0) = \eta_t + \sqrt{\beta}\eta_x\phi_x(x,0) + \sqrt{\beta}\eta\phi_{xx}(x,0) + O(\beta)$$

which is the same as

$$\phi_z(x,0) = \eta_t + \sqrt{\beta}(\eta\phi_x(x,0))_x + O(\beta).$$

Using Eq. (3.9) in the expression above,

$$\begin{aligned}\phi_z(x,0) &= \eta_t + \sqrt{\beta}\left(\eta\frac{1}{M(\xi)}\mathcal{T}[M(\tilde{\xi})\eta_t]\right)_x + O(\beta),\\ &= \eta_t + \frac{\sqrt{\beta}}{M(\xi)}\left(\eta\frac{1}{M(\xi)}\mathcal{T}[M(\tilde{\xi})\eta_t]\right)_\xi + O(\beta).\end{aligned}$$

Thus by means of the Hilbert transform on the corrugated strip,

$$\begin{aligned}\phi_x(x,0) &= \frac{1}{M(\xi)}\mathcal{T}[M(\tilde{\xi})\phi_z(x,0)],\\ &= \frac{1}{M(\xi)}\mathcal{T}\left[M(\tilde{\xi})\left(\eta_t + \frac{\sqrt{\beta}}{M(\tilde{\xi})}\left(\eta\frac{1}{M(\tilde{\xi})}\mathcal{T}[M(\xi')\eta_t]\right)_\xi\right)\right] + O(\beta),\\ &= \frac{1}{M(\xi)}\mathcal{T}\left[M(\tilde{\xi})\eta_t + \sqrt{\beta}\left(\eta\frac{1}{M(\tilde{\xi})}\mathcal{T}[M(\xi')\eta_t]\right)_\xi\right] + O(\beta).\end{aligned}$$

It is easy to take a time-derivative of this expression since the coefficient $M$ is independent of $t$:

$$\phi_{tx}(x,0) = \frac{1}{M(\xi)}\mathcal{T}\left[M(\tilde{\xi})\eta_t + \sqrt{\beta}\left(\eta\frac{1}{M(\tilde{\xi})}\mathcal{T}[M(\xi')\eta_t]\right)_\xi\right]_t + O(\beta),$$

which together with

$$\eta_{tt} = ((1-\eta)\overline{u_1})_{xt} = ((1-\eta)\overline{u_1})_{\xi t}/M(\xi)$$

leads to

$$\sqrt{\beta}\,\phi_{tx}|_{z=0} = \frac{\sqrt{\beta}}{M(\xi)}\mathcal{T}\left[((1-\eta)\overline{u_1})_{\xi t}\right] + \frac{\beta}{M(\xi)}\mathcal{T}\left[\frac{\eta}{M(\tilde{\xi})}\mathcal{T}\left[((1-\eta)\overline{u_1})_{\xi}\right]\right]_{\xi t} + O(\beta^{\frac{3}{2}}),$$

and as we saw

$$\begin{aligned}\frac{\beta}{2}\left(\phi_x^2|_{z=0}\right)_x &= \frac{\beta}{2}\left(\left\{\frac{1}{M(\xi)}\mathcal{T}[M(\tilde{\xi})\eta_t]\right\}^2\right)_x + O(\beta^{\frac{3}{2}}),\\ &= \frac{\beta}{2M(\xi)}\left(\left\{\frac{1}{M(\xi)}\mathcal{T}[M(\tilde{\xi})\eta_t]\right\}^2\right)_\xi + O(\beta^{\frac{3}{2}}),\\ &= \frac{\beta}{2M(\xi)}\left(\left\{\frac{1}{M(\xi)}\mathcal{T}\left[((1-\eta)\overline{u_1})_{\xi}\right]\right\}^2\right)_\xi + O(\beta^{\frac{3}{2}}).\end{aligned}$$

Summarizing, the higher order pressure term connecting the top and lower layer is

$$\begin{aligned}P_x(x,t) = -\frac{\rho_2}{\rho_1}\Bigg(&\eta_x + \frac{\sqrt{\beta}}{M(\xi)}\mathcal{T}\left[((1-\eta)\overline{u_1})_{\xi t}\right] +\\ &+ \frac{\beta}{M(\xi)}\mathcal{T}\left[\frac{\eta}{M(\xi)}\mathcal{T}\left[((1-\eta)\overline{u_1})_{\xi}\right]\right]_{\xi t} +\\ &+ \frac{\beta}{2M(\xi)}\left(\left\{\frac{1}{M(\xi)}\mathcal{T}\left[((1-\eta)\overline{u_1})_{\xi}\right]\right\}^2\right)_\xi +\\ &+ \frac{\beta}{M(\xi)}\left(\eta\eta_{tt} + \frac{1}{2}\eta_t^2\right)\Bigg) + O(\beta^{\frac{3}{2}}).\end{aligned}$$

This order of approximation is compatible with the nonhydrostatic corrections

added to the upper shallow water layer model since it makes the order $\beta$ terms explicit.

Notice that composition of the Hilbert operator $\mathcal{T}$ arises in this case. A similar situation also occurred in the fully dispersive Boussinesq model obtained by Matsuno in [19] and Artiles and Nachbin in [1] for surface gravity waves.

The above pressure term is substituted into the system of Eqs. (3.1) and (3.8) in curvilinear coordinates, that is,

$$\begin{cases} \eta_t = \dfrac{1}{M(\xi)}((1-\eta)\overline{u_1})_\xi, \\ \\ \overline{u_1}_t + \dfrac{1}{M(\xi)}\overline{u_1}\,\overline{u_1}_\xi = -\dfrac{1}{M(\xi)}\eta_\xi + \dfrac{\beta}{(1-\eta)}\dfrac{1}{3M(\xi)}((1-\eta)^3 G_1)_\xi - P_x + O(\beta^2) \end{cases}$$

where

$$G_1(\xi,t) = \frac{1}{M(\xi)}\overline{u_1}_{\xi t} + \frac{\overline{u_1}}{M(\xi)}\left(\frac{1}{M(\xi)}\overline{u_1}_\xi\right)_\xi - \frac{1}{M(\xi)^2}\overline{u_1}_\xi\overline{u_1}_\xi.$$

As a result, the strongly nonlinear model of order $\beta^{\frac{3}{2}}$ is:

$$\begin{cases} \eta_t = \dfrac{1}{M(\xi)}((1-\eta)\overline{u_1})_\xi, \\ \\ \overline{u_1}_t + \dfrac{1}{M(\xi)}\overline{u_1}\,\overline{u_1}_\xi + \dfrac{1}{M(\xi)}\left(1-\dfrac{\rho_2}{\rho_1}\right)\eta_\xi = \dfrac{\rho_2}{\rho_1}\dfrac{\sqrt{\beta}}{M(\xi)}\mathcal{T}\left[(1-\eta)\overline{u_1}\right]_{\xi t} + \\ \quad + \dfrac{\beta}{1-\eta}\dfrac{1}{3M(\xi)}\left((1-\eta)^3 G_1\right)_\xi + \dfrac{\rho_2}{\rho_1}\dfrac{\beta}{M(\xi)}\left(\dfrac{\eta((1-\eta)\overline{u_1})_{\xi t}}{M(\xi)} + \dfrac{1}{2}((1-\eta)\overline{u_1})_\xi^2\right)_\xi + \\ \quad + \dfrac{\beta}{M(\xi)}\dfrac{\rho_2}{\rho_1}\mathcal{T}\left[\dfrac{\eta}{M(\xi)}\mathcal{T}[(1-\eta)\overline{u_1}]_\xi\right]_{\xi t} + \\ \quad + \dfrac{\beta}{2M(\xi)}\dfrac{\rho_2}{\rho_1}\left(\left\{\dfrac{1}{M(\xi)}\mathcal{T}\left[((1-\eta)\overline{u_1})_\xi\right]\right\}^2\right)_\xi + O(\beta^{\frac{3}{2}}), \end{cases}$$

For the weakly nonlinear model of order $\beta^{\frac{3}{2}}$ introduce $\eta^*$, $\overline{u_1}^*$ such that

$$\eta = \alpha\eta^*, \qquad \overline{u_1} = \alpha\overline{u_1}^*,$$

with $\alpha = O\left(\sqrt{\beta}\right)$, a typical scaling used for solitary waves. After dropping the asterisks we have

$$\begin{cases} \eta_t = \dfrac{1}{M(\xi)}[(1-\alpha\eta)\overline{u_1}]_\xi, \\ \\ \overline{u_1}_t + \dfrac{\alpha}{M(\xi)}\overline{u_1}\,\overline{u_1}_\xi + \dfrac{1}{M(\xi)}\left(1-\dfrac{\rho_2}{\rho_1}\right)\eta_\xi = \dfrac{\rho_2}{\rho_1}\dfrac{\sqrt{\beta}}{M(\xi)}\mathcal{T}[(1-\alpha\eta)\overline{u_1}]_{\xi t} + \\ \quad + \dfrac{\beta}{3M(\xi)}\left(\dfrac{1}{M(\xi)}\overline{u_1}_{\xi t}\right)_\xi + O(\beta^{\frac{3}{2}}). \end{cases}$$

The higher-order weakly nonlinear model has exactly the same form as the lower-order strongly nonlinear model when the last term, namely,

$$\frac{\beta}{3M(\xi)}\left(\frac{1}{M(\xi)}\overline{u_1}_{\xi t}\right)_\xi$$

of the weakly nonlinear model is neglected. This implies that the weakly nonlinear higher-order model should serve as a good model for moderate amplitude internal waves in a deep water configuration. Furthermore, when the additional term from the upper layer is included, the linear dispersion relation for the higher-order weakly nonlinear model becomes the closest to the exact linear dispersion relation when compared to lower-order models, as will be shown in the next Section. In other words, the weakly nonlinear higher-order model might have a large domain of validity so that the model can be used for a moderate (although still large) ra-

tio of $h_2/h_1$, where the effects of bottom topography are more pronounced. This might be a justification for using a higher-order weakly nonlinear model and will be thoroughly explored in the near future.

## 3.3 Dispersion relation for the higher-order model. Comparison with the previous model

To obtain the dispersion relation for the improved model, consider its linearization around the undisturbed state so that

$$\begin{cases} \eta_t = \overline{u_1}_\xi, \\ \\ \overline{u_1}_t + \left(1 - \dfrac{\rho_2}{\rho_1}\right)\eta_\xi = \dfrac{\rho_2}{\rho_1}\sqrt{\beta}\,\mathcal{T}[\overline{u_1}]_{\xi t} + \dfrac{\beta}{3}\overline{u_1}_{\xi\xi t}, \end{cases}$$

in the presence of a flat bottom.

Taking derivatives once in $t$, $\eta$ can be eliminated from the second equation,

$$\overline{u_1}_{tt} + \left(1 - \frac{\rho_2}{\rho_1}\right)\overline{u_1}_{\xi\xi} - \frac{\rho_2}{\rho_1}\sqrt{\beta}\,\mathcal{T}[\overline{u_1}]_{\xi tt} - \frac{\beta}{3}\overline{u_1}_{\xi\xi tt} = 0.$$

Let $\overline{u_1} = Ae^{i(kx-\omega t)}$. Substituting above and using again that $\mathcal{T}[e^{ikx}] = i\coth\left(\frac{kh_2}{L}\right)e^{ikx}$ we get

$$\omega^2\left(1 + \frac{\beta}{3}k^2 + \frac{\rho_2}{\rho_1}\sqrt{\beta}\,k\coth\left(\frac{kh_2}{L}\right)\right) = \left(\frac{\rho_2}{\rho_1} - 1\right)k^2,$$

that is,

$$\omega^2 = \frac{\left(\frac{\rho_2}{\rho_1} - 1\right)k^2}{1 + \frac{\beta}{3}k^2 + \frac{\rho_2}{\rho_1}\sqrt{\beta}\,k\coth\left(\frac{kh_2}{L}\right)}. \tag{3.10}$$

Again, $\frac{\omega^2}{k^2} \to 0$ as $k \to \infty$, so bounded phase velocities are obtained as $k$ becomes large.

Now, let us make a comparison between the different dispersion relations obtained throughout this work. Initially, we have the dimensional full dispersion relation

$$\boldsymbol{\omega}_f^2 = \frac{g(\rho_2 - \rho_1)\mathbf{k}^2}{\rho_1 \mathbf{k}\coth(\mathbf{k}h_1) + \rho_2 \mathbf{k}\coth(\mathbf{k}h_2)} \tag{3.11}$$

that comes from the linearized Euler equations around the undisturbed state, see for example [18]. To compare it with the dimensionless dispersion relations (2.29) and (3.10) it must be taken into account that because of the non-dimensionalization,

$$\mathbf{k} = \frac{k}{L}, \qquad \boldsymbol{\omega} = \frac{U_0}{L}\omega.$$

Therefore, (2.29) in dimensional form becomes

$$\boldsymbol{\omega}_r^2 = \frac{g(\rho_2 - \rho_1)\mathbf{k}^2}{\frac{\rho_1}{h_1} + \rho_2 \mathbf{k}\coth(\mathbf{k}h_2)}. \tag{3.12}$$

As it has been stated, the reduced model (2.27) captures the dispersion relation for the shallow water (long waves) regime in the upper layer since

$$\rho_1 \mathbf{k}\coth(\mathbf{k}h_1) \to \frac{\rho_1}{h_1},$$

as $\mathbf{k}h_1 \to 0$.

On the other side, the relation (3.10) in dimensional form is

$$\boldsymbol{\omega}_h^2 = \frac{g(\rho_2 - \rho_1)\mathbf{k}^2}{\frac{\rho_1}{h_1} + \frac{1}{3}h_1\rho_1\mathbf{k}^2 + \rho_2 \mathbf{k}\coth(\mathbf{k}h_2)}.$$

Notice that both approaches are fully dispersive regarding the bottom layer, since the second coth is completely retained. For the shallow water upper layer regime ($\mathbf{k}h_1$ near zero) we obtain again the correct approximation of the full dispersion relation, but here the term $\rho_1 \mathbf{k} \coth(\mathbf{k}h_1)$ in the denominator is expanded with one more term, namely

$$\frac{\rho_1}{h_1}\mathbf{k}h_1 \coth(\mathbf{k}h_1) = \frac{\rho_1}{h_1}\left(1 + \frac{(\mathbf{k}h_1)^2}{3} + O\left((\mathbf{k}h_1)^4\right)\right),$$

and consequently

$$\boldsymbol{\omega}_f^2 = \boldsymbol{\omega}_h^2 + O\left((\mathbf{k}h_1)^4\right),$$

while

$$\boldsymbol{\omega}_f^2 = \boldsymbol{\omega}_r^2 + O\left((\mathbf{k}h_1)^2\right).$$

This means that the linear dispersion relation from the higher-order nonlinear model $\boldsymbol{\omega}_h^2$ is closer to the full (exact) linear dispersion relation $\boldsymbol{\omega}_f^2$ than the linear dispersion relation from the lower-order model $\boldsymbol{\omega}_r^2$ is. See Fig. 3.1 and a detail in Fig. 3.2 where the corresponding phase velocities are depicted.

The inclusion of the higher order pressure term has improved the accuracy of the phase speed over a much wider wavenumber band. This is very important in reflection-transmission problems as shown by Muñoz and Nachbin in [23].

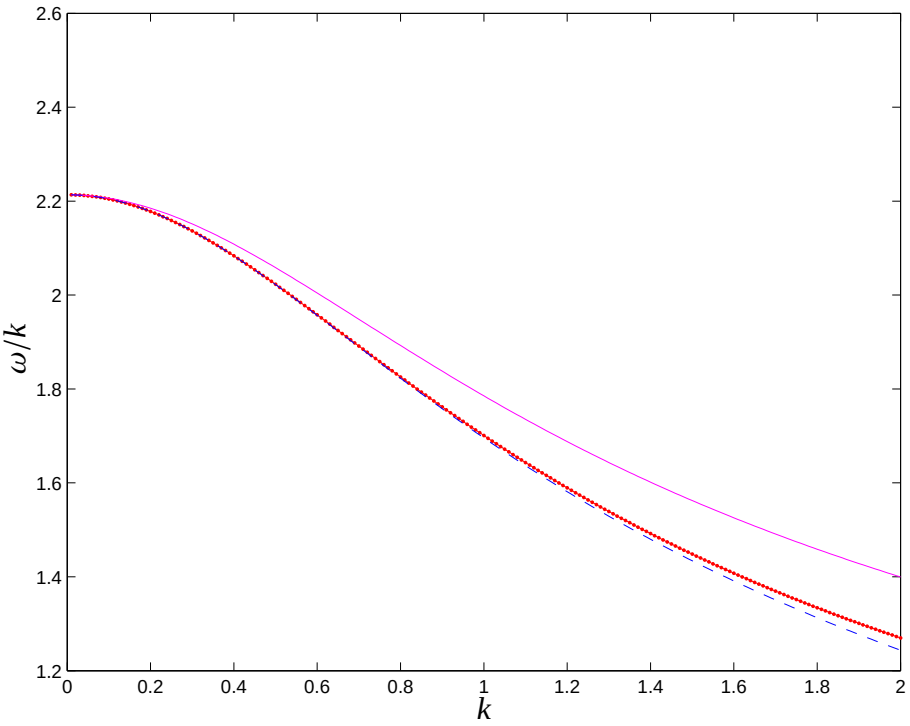


Figure 3.1: Phase velocities for $\rho_1 = 1$, $\rho_2 = 2$, $h_1 = 1$, $h_2 = 2$, $\beta = 0.01$. Dotted line: full phase velocity, dashed line: phase velocity for the higher order model, solid line: phase velocity for the lower order model.

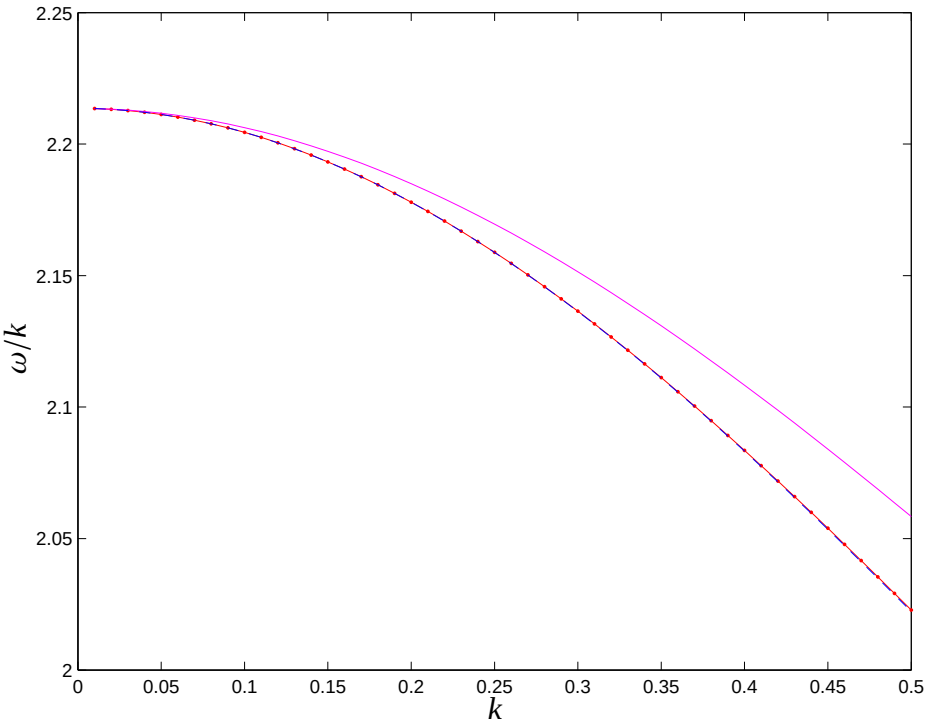


Figure 3.2: Detail from Fig. 3.1.

# Chapter 4

# Numerical results

## 4.1 Hierarchy of one-dimensional models

For numerical implementations, we first normalize the shallow water velocity $c_0^2 = \left(\frac{\rho_2}{\rho_1} - 1\right)$ of system (2.27) by setting $\eta = \eta^*$, $\overline{u_1} = c_0\overline{u_1}^*$, $t = \frac{t^*}{c_0}$. Dropping the asterisks, the following Strongly Nonlinear Corrugated Bottom Model (SNCM) is obtained,

$$\begin{cases} \eta_t - \dfrac{1}{M(\xi)}[(1-\eta)\overline{u_1}]_\xi = 0, \\ \overline{u_1}_t + \dfrac{1}{M(\xi)}\overline{u_1}\,\overline{u_1}_\xi - \dfrac{1}{M(\xi)}\eta_\xi = \sqrt{\beta}\dfrac{\rho_2}{\rho_1}\dfrac{1}{M(\xi)}\mathcal{T}_{[0,2\ell]}\,[(1-\eta)\overline{u_1}]_{\xi t}\,. \end{cases} \tag{4.1}$$

We will work on the periodic domain $\xi \in \Pi[0, 2\ell]$, so that instead of the operator $\mathcal{T}$ its periodic version $\mathcal{T}_{[0,2\ell]}$ appears above. See Appendix C for the definition of $\mathcal{T}_{[0,2\ell]}$. The choice of a computational periodic domain was made to be able to use spectral methods. To avoid the influence of the boundaries on the evolution of the perturbation $\eta$ interacting with the bottom profile we added two

homogeneuous (flat) regions at the extremes and keep the dynamics away from these regions. Hence both profile and initial disturbance will be defined and kept away from $\xi = 0 = 2\ell$.

From system (4.1), a hierarchy of one-dimensional models can be derived by considering the different regimes (linear, weakly nonlinear or strongly nonlinear) as well as the flat or corrugated bottom cases. The Weakly Nonlinear Corrugated Bottom Model (WNCM) was already obtained in (2.30). In curvilinear coordinates for a periodic domain it reads

$$\begin{cases} \eta_t - \dfrac{1}{M(\xi)}[(1-\alpha\eta)\overline{u_1}]_\xi = 0, \\ \overline{u_1}_t + \dfrac{\alpha}{M(\xi)}\overline{u_1}\,\overline{u_1}_\xi - \dfrac{1}{M(\xi)}\eta_\xi = \sqrt{\beta}\dfrac{\rho_2}{\rho_1}\dfrac{1}{M(\xi)}\mathcal{T}_{[0,2\ell]}[\overline{u_1}]_{\xi t}\,. \end{cases} \tag{4.2}$$

Setting $\alpha = 0$ we obtained the Linear Corrugated Bottom Model (LCM)

$$\begin{cases} \eta_t - \dfrac{1}{M(\xi)}\overline{u_1}_\xi = 0, \\ \overline{u_1}_t - \dfrac{1}{M(\xi)}\eta_\xi = \sqrt{\beta}\dfrac{\rho_2}{\rho_1}\dfrac{1}{M(\xi)}\mathcal{T}_{[0,2\ell]}[\overline{u_1}]_{\xi t}\,. \end{cases} \tag{4.3}$$

The flat bottom versions are obtained by simply taking $M(\xi) = 1$ for all $\xi \in \Pi[0, 2\ell]$. To fix a notation, let us use the abbreviations in Table 4.1 to refer to each model.

## 4.2 Method of lines

To find the solution for the initial value problem of systems SNCM, WNCM, SNFM, WNFM, LCM is a nontrivial task. That is why we resort to numerical methods to find approximate solutions.

| | Linear | Weakly non-linear | Strongly non-linear |
|---|---|---|---|
| Flat bottom | LFM | WNFM | SNFM |
| Rough bottom | LCM | WNCM | SNCM |

Table 4.1: Abbreviations for the six different models.

In order to use the method of lines to solve numerically the systems of equations (4.1, 4.2, 4.3) and their flat bottom versions, let us rewrite them in a more convenient way,

$$\begin{cases} \eta_t = E(\eta, \overline{u_1}), \\ V_t = F(\eta, \overline{u_1}), \end{cases} \tag{4.4}$$

where $V$ is an auxiliary variable defined for each model in Table 4.2. The corresponding vector field $(E, F)$ is defined in Table 4.3. The mean-layer horizontal upper velocity $\overline{u_1}$ can be recovered from $\eta$ and $V$ by inverting the relations in Table 4.2 in a way to be specified later on for each case. For the time being, let us assume that $\overline{u_1} = \Psi(\eta, V)$, given a certain operator $\Psi$.

According to the method of lines, we can discretize in space and solve a coupled system of ODEs by a finite difference formula in $t$ like, for example, a Runge-Kutta integration scheme or a predictor-corrector solver with an Adams-Bashforth predictor and an Adams-Moulton corrector.

First, an approximation scheme for the $\xi$-derivatives involved in the right-hand side of the systems above must be used for the discretization in space. A choice

| $V$ | Flat bottom | Rough bottom |
|---|---|---|
| Linear | $\overline{u_1} - \sqrt{\beta}\,\frac{\rho_2}{\rho_1}\mathcal{T}_{[0,2\ell]}\left[\overline{u_1}\right]_\xi$ | $\overline{u_1} - \sqrt{\beta}\,\frac{\rho_2}{\rho_1}\frac{1}{M(\xi)}\mathcal{T}_{[0,2\ell]}\left[\overline{u_1}\right]_\xi$ |
| Weakly Nonlinear | $\overline{u_1} - \sqrt{\beta}\,\frac{\rho_2}{\rho_1}\mathcal{T}_{[0,2\ell]}\left[\overline{u_1}\right]_\xi$ | $\overline{u_1} - \sqrt{\beta}\,\frac{\rho_2}{\rho_1}\frac{1}{M(\xi)}\mathcal{T}_{[0,2\ell]}\left[\overline{u_1}\right]_\xi$ |
| Strongly Nonlinear | $\overline{u_1} - \sqrt{\beta}\,\frac{\rho_2}{\rho_1}\mathcal{T}_{[0,2\ell]}\left[(1-\eta)\overline{u_1}\right]_\xi$ | $\overline{u_1} - \sqrt{\beta}\,\frac{\rho_2}{\rho_1}\frac{1}{M(\xi)}\mathcal{T}_{[0,2\ell]}\left[(1-\eta)\overline{u_1}\right]_\xi$ |

Table 4.2: The auxiliary variable $V$.

| $(E,F)$ | Flat bottom | Rough bottom |
|---|---|---|
| Linear | $\left(\overline{u_1}_\xi, \eta_\xi\right)$ | $\frac{1}{M(\xi)}\left(\overline{u_1}_\xi, \eta_\xi\right)$ |
| Weakly Nonlinear | $\left(\left[(1-\alpha\eta)\overline{u_1}\right]_\xi, \eta_\xi - \alpha\overline{u_1}\,\overline{u_1}_\xi\right)$ | $\frac{1}{M(\xi)}\left(\left[(1-\alpha\eta)\overline{u_1}\right]_\xi, \eta_\xi - \alpha\overline{u_1}\,\overline{u_1}_\xi\right)$ |
| Strongly Nonlinear | $\left(\left[(1-\eta)\overline{u_1}\right]_\xi, \eta_\xi - \overline{u_1}\,\overline{u_1}_\xi\right)$ | $\frac{1}{M(\xi)}\left(\left[(1-\eta)\overline{u_1}\right]_\xi, \eta_\xi - \overline{u_1}\,\overline{u_1}_\xi\right)$ |

Table 4.3: The field $(E,F)$.

is to approximate the $\xi$-derivative of a function $f(\xi)$ by the fourth order, five point formula

$$f_\xi(\xi_j) = \frac{8(f_{j+1} - f_{j-1}) + f_{j-2} - f_{j+2}}{12\Delta\xi} + O(\Delta\xi^4), \tag{4.5}$$

where $f_j = f(\xi_j)$, $\xi_j = j\Delta\xi$, $\Delta\xi = 2\ell/N$, $j = 1, \ldots, N$. So the spatial discretization for the LFM with $\beta = 0$ (which is just the wave equation) leads to the system of Ordinary Differential Equations (ODEs)

$$\begin{cases} \eta_t = C\overline{u_1}, \\ \overline{u_1}_t = C\eta, \end{cases}$$

where $\eta = [\eta_1, \ldots, \eta_N]^t$, with $\eta_j = \eta(j\Delta\xi, t)$ and $\overline{u_1} = [\overline{u_1}_1, \ldots, \overline{u_1}_N]^t$, with $\overline{u_1}_j = \overline{u_1}(j\Delta\xi, t)$, $j = 1, \ldots, N$. $C$ is the skew-symmetric, circulant matrix,

$$C = \frac{1}{\Delta\xi}\begin{bmatrix} 0 & 2/3 & -1/12 & 0 & \cdots & 0 & 1/12 & -2/3 \\ -2/3 & 0 & 2/3 & -1/12 & & & \ddots & 1/12 \\ 1/12 & -2/3 & 0 & 2/3 & \ddots & & & 0 \\ 0 & 1/12 & -2/3 & 0 & \ddots & \ddots & & \\ \vdots & & \ddots & \ddots & \ddots & \ddots & \ddots & \\ 0 & & & \ddots & \ddots & 0 & 2/3 & -1/12 \\ -1/12 & \ddots & & & \ddots & -2/3 & 0 & 2/3 \\ 2/3 & -1/12 & 0 & & & 1/12 & -2/3 & 0 \end{bmatrix}.$$

Since it is a skew-symmetric matrix, it has imaginary eigenvalues. The same is true for the block matrix

$$\left[\begin{array}{c|c} & C \\ \hline C & \end{array}\right],$$

which has the same eigenvalues of $C$ with double multiplicity.

Another choice to approximate the $\xi$-derivatives is to use the spectral $\xi$-derivative, whose corresponding matrix is

$$D = \begin{bmatrix} 0 & & & & -\frac{1}{2}\cot(\frac{1\Delta\xi}{2}) \\ -\frac{1}{2}\cot(\frac{1\Delta\xi}{2}) & \ddots & \ddots & & \frac{1}{2}\cot(\frac{2\Delta\xi}{2}) \\ \frac{1}{2}\cot(\frac{2\Delta\xi}{2}) & & \ddots & & -\frac{1}{2}\cot(\frac{3\Delta\xi}{2}) \\ -\frac{1}{2}\cot(\frac{3\Delta\xi}{2}) & & \ddots & & \vdots \\ \vdots & & \ddots & \ddots & -\frac{1}{2}\cot(\frac{(N-1)\Delta\xi}{2}) \\ -\frac{1}{2}\cot(\frac{(N-1)\Delta\xi}{2}) & & & & 0 \end{bmatrix}.$$

Here we also have a skew-symmetric, Toeplitz, circulant matrix with imaginary eigenvalues $ik$, $k = -N/2 + 1, \ldots, N/2 - 1$, with zero having multiplicity 2. With it, the discretization of the non-dispersive LFM leads to an ODEs system for $\eta$ and $\overline{u_1}$ involving the block matrix

$$\left[\begin{array}{c|c} & D \\ \hline D & \end{array}\right].$$

This block matrix has the same imaginary eigenvalues of $D$ with double multiplicity.

The rule of thumb for stability (valid for normal matrices) is [28]: the method of lines is stable if the eigenvalues of the linearized spatial discretization operator, scaled by $\Delta t$, lie in the stability region of the time-discretization operator.

In Fig. 4.1 we depict the stability regions for the fourth order Runge-Kutta integration scheme (RK4), the fifth order, four step Adams-Moulton scheme (AM4) and the fourth order, three step Adams-Moulton scheme (AM3). Along the imag-

inary axis (where the eigenvalues of the linearized spatial discretization operators lie), RK4 is less restrictive, allowing larger time steps and numerical evolution over longer time intervals, as we will see in the experiments below. For a better visualization, in Fig. 4.2 we compute the amplification factor $|R(z)|$ where $z = \lambda\Delta t$ and $\lambda$ represents the largest (in the sense of absolute value) eigenvalue of the linearized spatial discretization operator, see for example [2]. The AM3 scheme has the smallest stability interval along the imaginary axis since the amplification factor becomes greater than one very quickly. This implies a more restrictive stability condition when using the AM3 scheme to solve the bidirectional wave equation, for example. However, for the regularized dispersive systems considered here, we obtained less instability since the phase velocity actually decreases as the wavenumber grows accommodating high wave-numbers better than in the hyperbolic case (see the dispersion relation in Section 2.3). Dispersion comes in as a physical regularization in comparison with its underlying hyperbolic counterpart. Still, the classical fourth order Runge-Kutta seems to be the best choice.

The spectral approximation of the $\xi$-derivative is more accurate than the five point formula exhibited above. However, we cannot use numerical velocity one ($\Delta t = \Delta\xi$) with it, in correspondence with the theoretical velocity, because of stability restrictions of the method of lines already discussed. The reason for choosing the Courant number as one is to avoid a numerical delay of the travelling wave speed that could interfere with the expected delay that may result from the interaction of the wave with a rapidly-varying bottom profile. This particular issue will be investigated in the near future. For the time being, we choose the five point formula (4.5) in all the numerical experiments presented in this chapter.

The time domain is discretized as $t_n = n\Delta t$, $n = 0, \ldots, T_{\text{final}}$ with $\Delta t = \Delta\xi$.

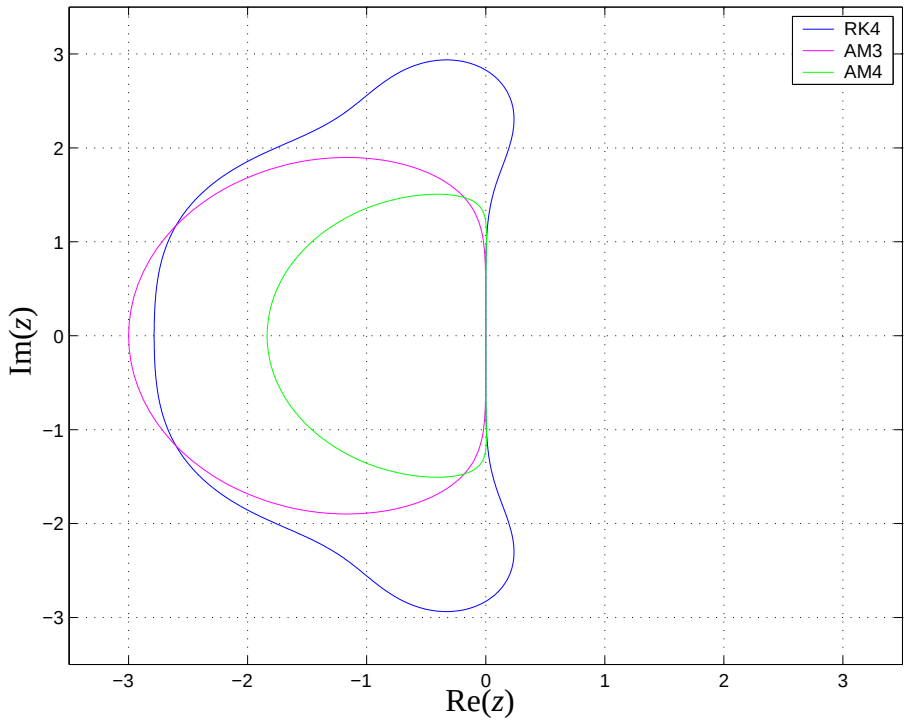


Figure 4.1: Stability regions for RK4, AM4, AM3.

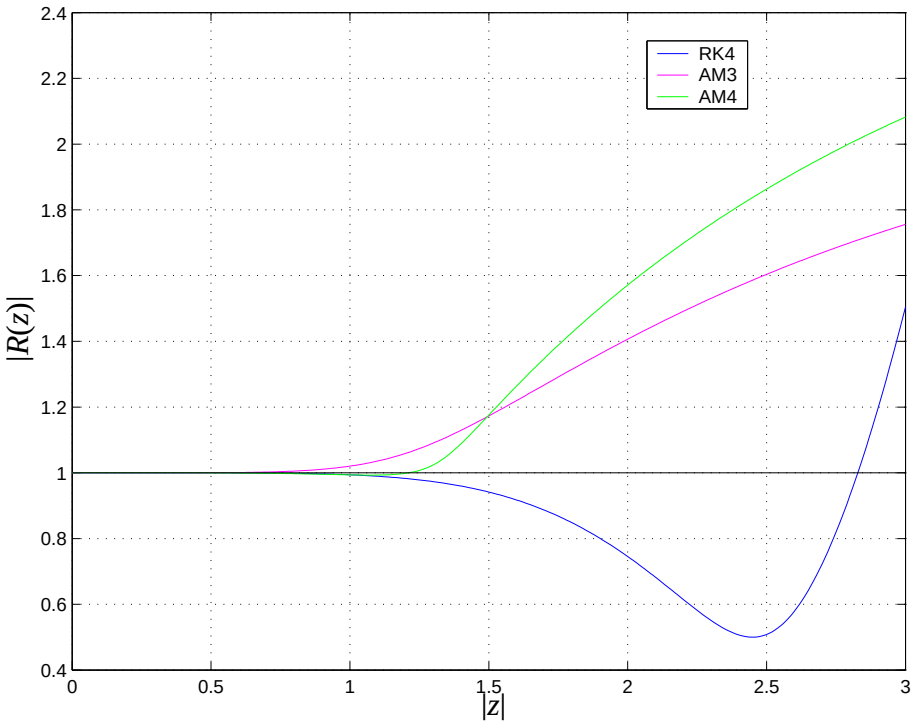


Figure 4.2: Amplification factor along the imaginary axis for RK4, AM3, AM4.

So the numerical velocity equals the theoretical one in the LFM above and the Courant number $\sigma = 1 \times \Delta t/\Delta\xi$ equals one. This choice is maintained throughout the numerical experiments with the different systems.

The time evolution step for $\eta$ and $V$ using RK4 is

$$\eta^{n+1} = \eta^n + \frac{\Delta t}{6}(K1 + 2K2 + 2K3 + K4)$$

$$V^{n+1} = V^n + \frac{\Delta t}{6}(KK1 + 2KK2 + 2KK3 + KK4),$$

where $\eta^n$ and $V^n$ are $N \times 1$ vectors with components $\eta_j^n = \eta(j\Delta\xi, n\Delta t)$ and $V^n = V(j\Delta\xi, n\Delta t)$ respectively. After each evolution step the $N \times 1$ vector $\overline{u_1}^n$ with components $\overline{u_1}_j^n = \overline{u_1}(j\Delta\xi, n\Delta t)$ must be recovered from $\eta^n$ and $V^n$ via $\overline{u_1}^n = \Psi(\eta^n, V^n)$.

Also, recall that

$$
\begin{aligned}
K1 &= E(\eta^n, \overline{u_1}^n),\\
KK1 &= F(\eta^n, \overline{u_1}^n),\\
\overline{u_1}_{k1} &= \Psi(\eta^n + 0.5\Delta t K1, V^n + 0.5\Delta t KK1),\\
K2 &= E(\eta^n + 0.5\Delta t K1, \overline{u_1}_{k1}),\\
KK2 &= F(\eta^n + 0.5\Delta t K1, \overline{u_1}_{k1}),\\
\overline{u_1}_{k2} &= \Psi(\eta^n + 0.5\Delta t K2, V^n + 0.5\Delta t KK2),\\
K3 &= E(\eta^n + 0.5\Delta t K2, \overline{u_1}_{k2}),\\
KK3 &= F(\eta^n + 0.5\Delta t K2, \overline{u_1}_{k2}),\\
\overline{u_1}_{k3} &= \Psi(\eta^n + \Delta t K3, V^n + \Delta t KK3),\\
K4 &= E(\eta^n + \Delta t K3, \overline{u_1}_{k3}),\\
KK4 &= F(\eta^n + \Delta t K3, \overline{u_1}_{k3}).
\end{aligned}
$$

Notice that the projection from $(\eta, V)$ back to $\overline{u_1}$ must be done after each stage. These intermediate values are denoted by $\overline{u_1}_{ki}$, $i = 1, 2, 3$.

Now we will specify how to deal with the operator $\Psi$ in order to recover $\overline{u_1}$ in terms of $V$ and $\eta$. Since the Fast Fourier Transform (FFT) of a Hilbert transform is easily computed, as well as the FFT for a $\xi$-derivative, we can go to frequency space and solve $\overline{u_1}$ in terms of $V$ for the linear and constant coefficients relation that appears in Table 4.2 for both LFM and WNFM. In Fourier space we have

$$
\widehat{V}(k) = \left(1 + \sqrt{\beta}\frac{\rho_2}{\rho_1}\frac{k\pi}{\ell}\coth\left(\frac{k\pi h_2}{\ell L}\right)\right)\widehat{\overline{u_1}}(k)
$$

for $k = -N/2+1, \ldots, N/2$. Therefore,

$$\widehat{\overline{u_1}}(k) = \frac{\widehat{V}(k)}{\left(1 + \sqrt{\beta}\frac{\rho_2}{\rho_1}\frac{k\pi}{\ell}\coth\left(\frac{k\pi h_2}{\ell L}\right)\right)},$$

since the denominator is always different from zero.

The remaining models are essentially different from the previous ones, as well as from the terrain following Boussinesq system obtained in [24] and solved numerically in [22] and the extended Boussinesq equations derived by Nwogu and solved numerically in [29]. This is due to the fact that in the present work, either the dispersive term has a nonlinear dependence between $\eta$ and $\overline{u_1}$, or it has a variable coefficient accompanying it. The use of the FFT is no longer straightforward, so we use a matrix formulation to find $\overline{u_1}^n$ in terms of $V^n$ and $\eta$.

For the SNCM (4.1) we have

$$V = \overline{u_1} - \sqrt{\beta}\frac{\rho_2}{\rho_1}\frac{1}{M(\xi)}\mathcal{T}_{[0,2\ell]}\left[(1-\eta)\overline{u_1}\right]_\xi . \tag{4.6}$$

Note a nonlinear term with the $\mathcal{T}$ operator and also a variable coefficient in front of it. The discrete version in matrix form of Eq. (4.6) reads

$$V = \left(\mathbf{1} - \sqrt{\beta}\frac{\rho_2}{\rho_1}M^{-1}TDA\right)\overline{u_1}, \tag{4.7}$$

where the $N \times N$ matrices involved are

- $M_{jj} = M(\xi_j)$, and zero elsewhere,
- $A_{jj} = 1 - \eta(\xi_j)$, and zero elsewhere,
- $D$ is the Fourier spectral spatial differentiation matrix,

- $T$ is the convolution matrix for $\mathcal{T}_{[0,2\ell]}$. The composition of convolution and differentiation can be computed with the help of the Fourier transform matrix $F$,

$$F_{jl} = w^{(j-1)(l-1)}, \qquad w = e^{2\pi i/N},$$

leading to the operator with symbol matrix

$$\Lambda_{ij} = \begin{cases} -\frac{j\pi}{\ell}\coth\left(\frac{j\pi h_2}{\ell L}\right), & i = j = 1, \ldots, N/2, \\ -\frac{(j-N)\pi}{\ell}\coth\left(\frac{(j-N)\pi h_2}{\ell L}\right), & i = j = N/2+1, \ldots, N-1, \\ 0 & \text{elsewhere,} \end{cases}$$

where

$$TD = DT = \frac{1}{N} F \Lambda \overline{F}.$$

Although the original expression (4.6) is nonlinear, the relation (4.7) is a linear algebraic system to be solved for $\overline{u_1}$ since $\eta$ and $V$ are already known at the current time step $n+1$. So at this stage, by using a spectral matrix instead of an FFT, we are only paying a price in complexity but not in accuracy. Table 4.4 sumarizes the discretizations used for each model, including the discretizations for the LFM and WNFM cases. These cases were implemented with the help of the FFT and also using a matrix formulation as a way to validate the method for the other models.

We also implemented in Matlab two predictor-corrector schemes, one that uses a third order, three step, explicit Adams-Bashforth solver (AB3) as predictor and a fourth order, three step implicit Adams-Moulton (AM3) as corrector. The other scheme uses a fourth order, four step Adams-Bashforth solver (AB4) as predictor and a fifth order, four step implicit Adams-Moulton (AM4) as corrector.

| $V$ | Flat bottom | Rough bottom |
|---|---|---|
| Linear | $\left(\mathbf{1} - \sqrt{\beta}\frac{\rho_2}{\rho_1}TD\right)\overline{u_1}$ | $\left(\mathbf{1} - \sqrt{\beta}\frac{\rho_2}{\rho_1}M^{-1}TD\right)\overline{u_1}$ |
| Weakly Nonlinear | $\left(\mathbf{1} - \sqrt{\beta}\frac{\rho_2}{\rho_1}TD\right)\overline{u_1}$ | $\left(\mathbf{1} - \sqrt{\beta}\frac{\rho_2}{\rho_1}M^{-1}TD\right)\overline{u_1}$ |
| Strongly Nonlinear | $\left(\mathbf{1} - \sqrt{\beta}\frac{\rho_2}{\rho_1}TDA\right)\overline{u_1}$ | $\left(\mathbf{1} - \sqrt{\beta}\frac{\rho_2}{\rho_1}M^{-1}TDA\right)\overline{u_1}$ |

Table 4.4: Discretizations for the relations in Table 4.2.

The AB3 scheme used is:

$$\eta_j^{n+1} = \eta_j^n + \frac{\Delta t}{12}(23E_j^n - 16E_j^{n-1} + 5E_j^{n-2}),$$

$$\overline{u_1}_j^{n+1} = \overline{u_1}_j^n + \frac{\Delta t}{12}(23F_j^n - 16F_j^{n-1} + 5F_j^{n-2}),$$

where $E_j^n = E(j\Delta\xi, n\Delta t)$ and $F_j^n = F(j\Delta\xi, n\Delta t)$. The AM3 scheme used is:

$$\eta_j^{n+1} = \eta_j^n + \frac{\Delta t}{24}(9E_j^{n+1} + 19E_j^n - 5E_j^{n-1} + E_j^{n-2}),$$

$$\overline{u_1}_j^{n+1} = \overline{u_1}_j^n + \frac{\Delta t}{24}(9F_j^{n+1} + 19F_j^n - 5F_j^{n-1} + F_j^{n-2}).$$

The AB4 scheme used is:

$$\eta_j^{n+1} = \eta_j^n + \frac{\Delta t}{24}(55E_j^n - 59E_j^{n-1} + 37E_j^{n-2} - 9E_j^{n-3}),$$

$$\overline{u_1}_j^{n+1} = \overline{u_1}_j^n + \frac{\Delta t}{24}(55F_j^n - 59F_j^{n-1} + 37F_j^{n-2} - 9F_j^{n-3}),$$

The AM4 scheme used is:

$$\eta_j^{n+1} = \eta_j^n + \frac{\Delta t}{720}(251E_j^{n+1} + 646E_j^n - 264E_j^{n-1} + 106E_j^{n-2} - 19E_j^{n-3}),$$

$$\overline{u_1}_j^{n+1} = \overline{u_1}_j^n + \frac{\Delta t}{720}(251F_j^{n+1} + 646F_j^n - 264F_j^{n-1} + 106F_j^{n-2} - 19F_j^{n-3}).$$

To initialize both predictor-corrector schemes, the RK4 described above is employed.

## 4.3 Flat bottom experiments

**Example 4.1.** We first consider the LFM for the non dispersive case $\beta = 0$,

$$\begin{cases} \eta_t = \overline{u_1}_\xi, \\ \overline{u_1}_t = \eta_\xi. \end{cases} \tag{4.8}$$

This is just the bidirectional wave equation for $\eta$

$$\eta_{tt} - \eta_{\xi\xi} = 0$$

with initial contidions

$$\begin{cases} \eta(\xi, 0) = \eta_0(\xi), \\ \eta_t(\xi, 0) = \overline{u_1}_{0\xi}(\xi). \end{cases}$$

This model (whose exact solution is well known) is useful for validating and comparing the numerical schemes, since it is more demanding than the dispersive models regarding numerical stability, as we commented in the previous Section.

Consider the initial condition

$$\eta_0(\xi) = 0.5e^{-a(\xi-2\pi)^2/64}, \qquad \xi \in \Pi[0, 16\pi],$$

with $a = 50$, $\eta_t(\xi, 0) = \overline{u_1}_{0\xi}(\xi) = -\eta_{0\xi}(\xi)$, where $\Pi[0, 16\pi]$ is the interval $[0, 16\pi]$ with periodic boundary conditions. If we set $\overline{u_1}$ initially to $-\eta_0(\xi)$ then the Riemann invariants for the nondispersive LFM, $A = \eta + \overline{u_1}$ and $B = \eta - \overline{u_1}$, will be $A(\xi, t) = 0$ and $B(\xi, t) = \eta(\xi - t, 0)$. Therefore

$$\eta = \frac{A + B}{2} = \eta(\xi - t, 0)$$

will be a right-travelling wave as shown in Fig. 4.3, where the numerical solution obtained with the AM4 scheme is shown until time $t = 39.2699$. The solution for the final time is also plotted in Fig. 4.4, the absolute error is 0.00098872, a little less than with RK4 (0.0013). Nevertheless, with RK4 we are able to advance much more in time, until $t = 151.1891$, while with AM4 instabilities set for $t = 49.0874$. AM3 is unstable as early as $t = 9.8175$.

**Example 4.2.** Another interesting example from the wave equation is that of the fission of the wave. Take the initial condition for $\eta$ as

$$\eta_0(\xi) = 0.5e^{-50(\xi-8\pi)^2/64}, \qquad \xi \in \Pi[0, 16\pi],$$

and $\overline{u_{10}} = 0$. If we set $\overline{u_1}$ initially to zero then the Riemann invariants will be $A(\xi, t) = \eta(\xi + t, 0)$ and $B(\xi, t) = \eta(\xi - t, 0)$. Therefore

$$\eta = \frac{A + B}{2} = \frac{\eta(\xi + t, 0) + \eta(\xi - t, 0)}{2}$$

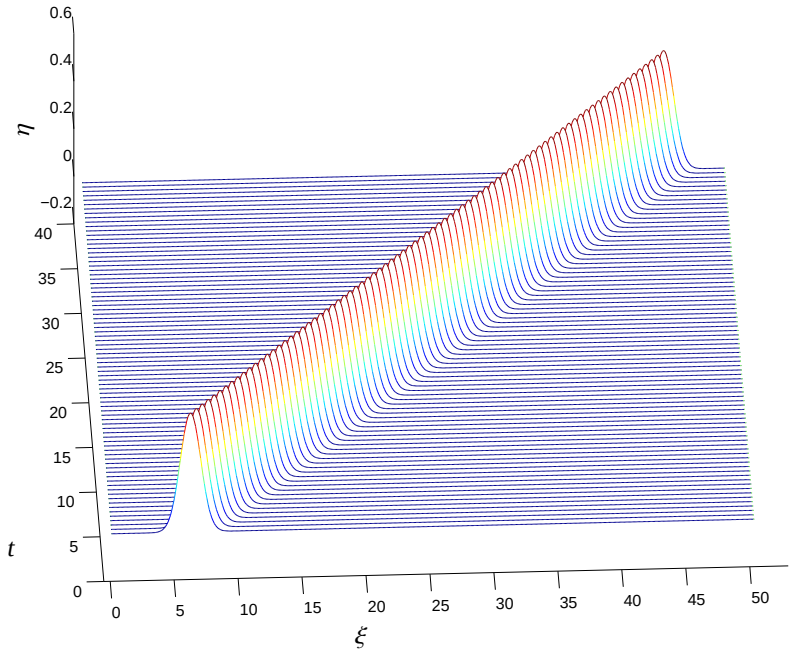


Figure 4.3: Travelling wave on a periodic domain $\Pi[0, 16\pi]$. The numerical solution was obtained using AM4 with $N = 512$, $\Delta\xi = 2\pi/N = 0.098175$, $\Delta t = \Delta\xi = 0.098175$.

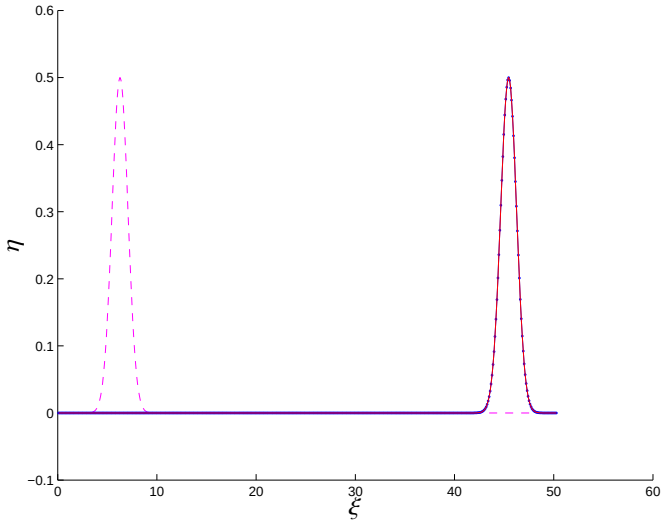


Figure 4.4: Travelling wave. Dotted line: numerical solution for the nondispersive LFM using AM4 for $t = 39.2699$ and $N = 512$, $\Delta\xi = 2l/N = 0.098175$, $\Delta t = \Delta\xi = 0.098175$, dashed line: initial condition, solid line: exact solution.

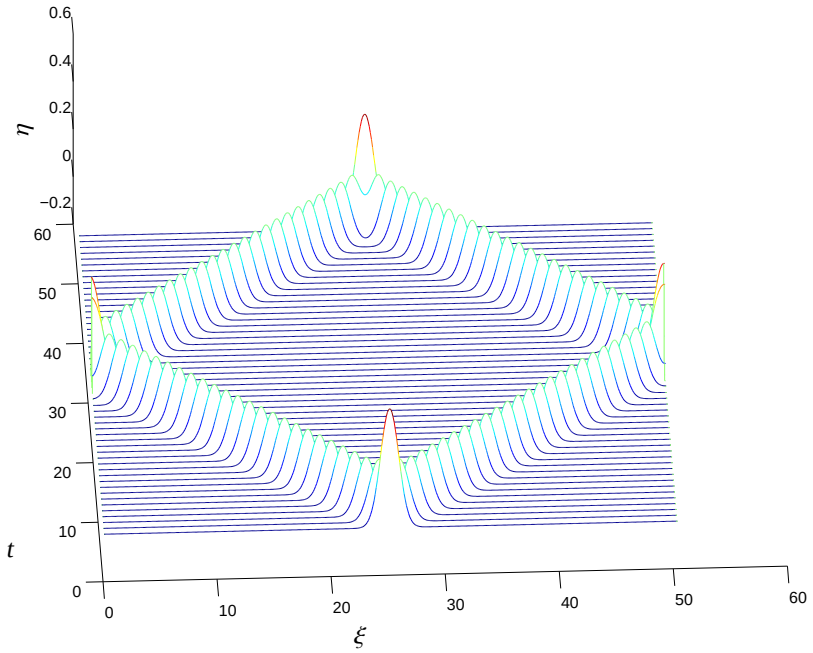


Figure 4.5: Fission of the wave on a periodic domain $\Pi[0, 16\pi]$.

and the amplitude is half of the original one, see Fig. (4.5). This is consistent with D'Alembert's solution for the wave equation. When the two travelling waves coincide (overlap) in space and time the initial condition is recovered with an error of 0.00374 by the RK4 method with $N = 512$, $\Delta\xi = 2l/N = 0.098175$, $\Delta t = \Delta\xi = 0.098175$, see Fig. 4.6. This is a nice consistency check for the numerical conservation of mass of two waves colliding.

**Example 4.3.** Let us study the numerical solutions for the LFM for the dispersive case $\beta \neq 0$. The initial value problem for this case can be solved explicitly by means of Fourier Series as follows.

Consider the initial value problem (IVP) for the LFM on the periodic domain

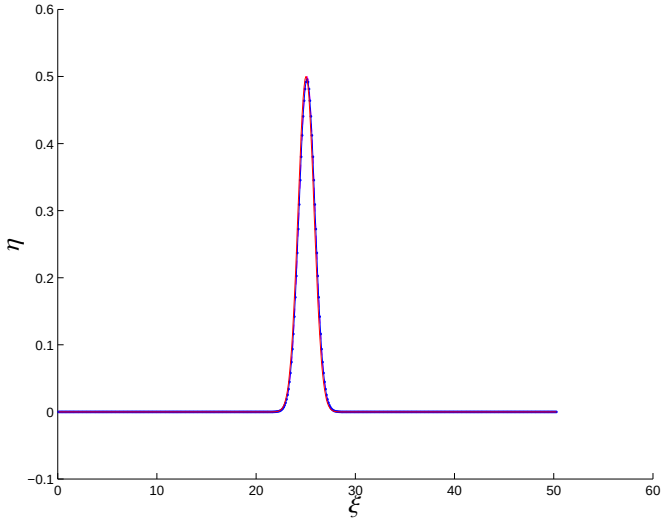


Figure 4.6: Fission of the wave. Dotted line: numerical solution for the nondispersive LFM using RK4 for $t = 50.2655$ and $N = 512$, $\Delta\xi = 2l/N = 0.098175$, $\Delta t = \Delta\xi = 0.098175$, dashed line: initial condition, solid line: exact solution.

$\xi \in \Pi[0, 2\ell]$,

$$\begin{cases} \eta_t - \overline{u_1}_\xi = 0, \\ \overline{u_1}_t - \eta_\xi = \sqrt{\beta}\dfrac{\rho_2}{\rho_1}\mathcal{T}_{[0,2\ell]}\left[\overline{u_1}\right]_{\xi t}, \\ \eta(\xi, 0) = \eta_0(\xi), \\ \overline{u_1}(\xi, 0) = \overline{u_1}_0(\xi). \end{cases} \tag{4.9}$$

First, let us perform the change of variables $\bar{\xi} = \pi\xi/\ell$, $\bar{t} = \pi t/\ell$ to the standard periodic domain $\xi \in \Pi[0, 2\pi]$. The time variable is modified in order to maintain the wave velocity as one for the hyperbolic regime ($\beta = 0$). In these coordinates

the IVP reads

$$\begin{cases} \eta_{\bar{t}} - \overline{u_1}_{\bar{\xi}} = 0, \\ \overline{u_1}_{\bar{t}} - \eta_{\bar{\xi}} = \sqrt{\beta}\dfrac{\rho_2}{\rho_1}\mathcal{T}_{[0,2\ell]}\left[\overline{u_1}\right]_{\bar{\xi}\bar{t}}, \\ \eta(\bar{\xi},0) = \eta_0(\bar{\xi}), \\ \overline{u_1}(\bar{\xi},0) = \overline{u_1}_0(\bar{\xi}). \end{cases} \tag{4.10}$$

The symbol of the operator $\mathcal{T}_{[0,2\ell]}[\cdot]_{\xi}$ (that is the composition of one spatial derivative with the Hilbert transform) in the new coordinates is

$$-\frac{k\pi}{\ell}\coth\left(\frac{k\pi}{\ell}\frac{h_2}{L}\right),$$

see Appendix C. Applying Fourier Transform (see Appendix C, Eq. (C.2) for its definition) to problem (4.10) we have

$$\begin{cases} \hat{\eta}_{\bar{t}} = ik\widehat{\overline{u_1}}, \\ \widehat{\overline{u_1}}_{\bar{t}}\left(1 + \sqrt{\beta}\dfrac{\rho_2}{\rho_1}\dfrac{k\pi}{\ell}\coth\left(\dfrac{k\pi}{\ell}\dfrac{h_2}{L}\right)\right) = ik\hat{\eta}, \quad \text{for } k \neq 0 \\ \hat{\eta}(k,0) = \widehat{\eta_0}(k), \\ \overline{u_1}(k,0) = \widehat{\overline{u_1}_0}(k). \end{cases} \tag{4.11}$$

Substitute $\widehat{\overline{u_1}}$ from the first equation into the second:

$$\hat{\eta}_{\bar{t}\bar{t}} = -\frac{k^2}{1 + \sqrt{\beta}\frac{\rho_2}{\rho_1}\frac{k\pi}{\ell}\coth\left(\frac{k\pi}{\ell}\frac{h_2}{L}\right)}\hat{\eta} = -\omega^2(k)\hat{\eta}.$$

The general solution for this ODE is

$$\hat{\eta}(k,t) = c_1\exp(i\omega(k)t) + c_2\exp(-i\omega(k)t), \quad k \neq 0,$$

where $c_1$ and $c_2$ are two functions of the wavenumber $k$. Using Fourier Series we can write the general solution for $\eta$, at least in a formal manner, as

$$\eta(\bar{\xi}, t) = \frac{1}{2\pi}\sum_{k=-\infty}^{\infty} c_1(k)\exp(i\omega(k)t)e^{ik\bar{\xi}} + \frac{1}{2\pi}\sum_{k=-\infty}^{\infty} c_2(k)\exp(-i\omega(k)t)e^{ik\bar{\xi}}.$$

Each term represents one wave mode, see [30]. Since the dispersion relation $\omega(k)$ is odd, each wave propagates in one direction: the first wave travels to the left, the second one to the right. Returning to Fourier space, from the initial condition in (4.11) we have,

$$\begin{cases} c_1(k) + c_2(k) = \widehat{\eta_0}(k), \\ c_1(k) - c_2(k) = \dfrac{k}{\omega(k)}\widehat{\overline{u_1}_0}(k). \end{cases} \tag{4.12}$$

Therefore,

$$c_1(k) = 0.5\left(\widehat{\eta_0}(k) + \frac{k}{\omega(k)}\widehat{\overline{u_1}_0}(k)\right)$$

and

$$c_2(k) = 0.5\left(\widehat{\eta_0}(k) - \frac{k}{\omega(k)}\widehat{\overline{u_1}_0}(k)\right).$$

For one propagation direction we set $c_1 = 0$, then

$$2c_1 = \widehat{\eta_0}(k) + k\widehat{\overline{u_1}_0}(k)/\omega(k) = 0,$$

which implies the following relation between each amplitude of the initial condition for $\overline{u_1}$ and the amplitude of the initial condition for $\eta$:

$$\widehat{\overline{u_1}_0}(k) = -\frac{\omega(k)}{k}\widehat{\eta_0}(k), \quad k \neq 0.$$

We use this relation to provide the initial condition for $\overline{u_1}_0$ (by means of an FFT)

for $\eta$ to propagate in only one direction. Moreover, $c_2(k) = \widehat{\eta_0}(k) = \hat{\eta}(k, 0)$. The exact solution is

$$\hat{\eta}(k,t) = \begin{cases} \widehat{\eta_0}(0), & k = 0, \\ \widehat{\eta_0}(k)\exp(-i\omega(k)t), & k \neq 0. \end{cases}$$

Although the amplitude of each mode is preserved as time advances, each component of the wavetrain travels with its own phase velocity $\omega(k)/k$. As a result, an initial Gaussian shape will disperse into an oscillatory train as shown in the numerical experiments. The exact solution can be employed to test the numerical scheme precision and stability properties. We consider the following Gaussian function as the initial perturbation of the interface,

$$\eta_0(\xi) = 0.5e^{-a(\xi-4\pi)^2/128}$$

with $a = 50$. The LFM parameters are $\ell = 16\pi$, $\rho_1 = 1$, $\rho_2 = 2$, $\beta = 0.05$, $\alpha = 0$. The numerical parameters are $N = 256$, $\Delta\xi = 2\ell/N = 0.3927$, $\Delta t = \Delta\xi = 0.3927$ . See Fig. 4.7 were the numerical solution for $t = 78.5398$ is depicted together with the initial condition. The numerical solution shows very good agreement with the exact solution. The same experiment with a finer grid, $N = 512$, $\Delta\xi = 2\ell/N = 0.19635$, $\Delta t = \Delta\xi = 0.19635$ is depicted in Fig. 4.8. The result is the same as the one obtained in the first experiment, which indicates convergence of the numerical method.

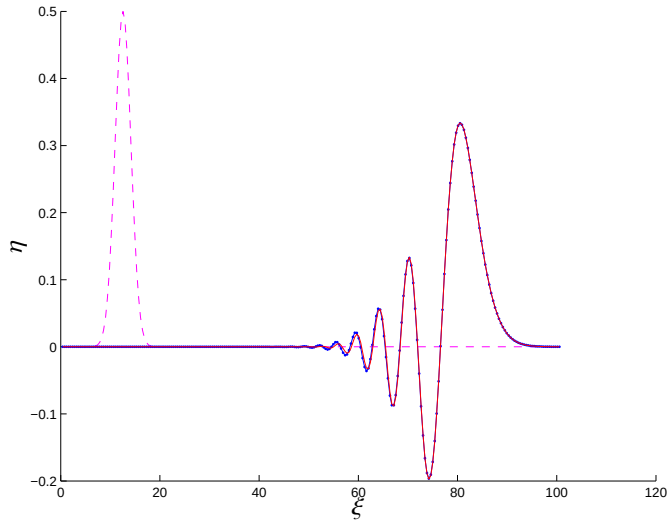


Figure 4.7: Pulse propagating over a flat bottom in the linear dispersive regime. Dotted line: numerical solution for the LFM using RK4 for $t = 78.5398$ and $N = 256$, dashed line: initial condition, solid line: exact solution.

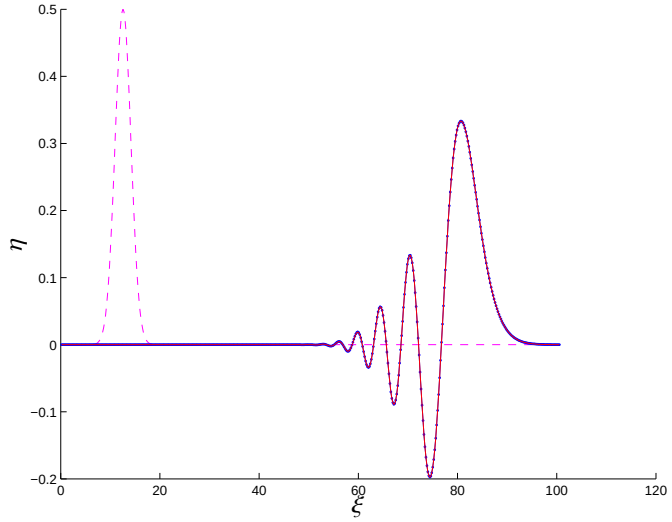


Figure 4.8: Pulse propagating over a flat bottom in the linear dispersive regime. Dotted line: numerical solution for the LFM using RK4 for $t = 78.5398$ and $N = 512$, dashed line: initial condition, solid line: exact solution.

## 4.4 Periodic topography experiments

When the bottom is flat, the topography dependent coefficient $M(\xi)$ is identically one. For the time being, we avoid the computation of $M(\xi)$ from the variable depth bottom, which can be costly even using Driscoll's package [10]. Let us assume that it is a function of the form $M(\xi) = 1 + n(\xi)$ where $n(\xi)$ describes periodic fluctuations. This choice is not far from the real coefficient that comes from mapping a periodic piecewise linear topography, see [21, 24, 22]. This strategy will prove useful for testing the models and observing the phenomena we are interested in.

**Example 4.4.** As a first example of a rough bottom let us consider a periodic slowly-varying coefficient $M(\xi)$ defined on the domain $[0, 16\pi]$ as

$$M(\xi) = \begin{cases} 1 + 0.5\sin(5\xi), & \text{for } 6\pi \leq \xi \leq 12\pi, \\ 1, & \text{elsewhere.} \end{cases}$$

The bottom irregularities are located in the region $6\pi \leq \xi \leq 12\pi$. There are 15 oscillations. The period of the bottom irregularities is $l = 1.2566$. The initial perturbation of the interface is the Gaussian function

$$\eta_0(\xi) = 0.5e^{-a(\xi-\pi)^2/64}$$

with $a = 200$, therefore its effective width is $L = 2.4$ and the ratio inhomogeneities/wavelength is about 0.5236. For the mean velocity $\overline{u_1}$ we choose the corresponding initial condition that gives one propagation direction for the LFM with $\beta = 0.0001$, $\alpha = 0$, as done in Section 4.3. See Fig. 4.9 where the numerical solution for $t = 36.3247$ is depicted together with the solution for the flat bottom

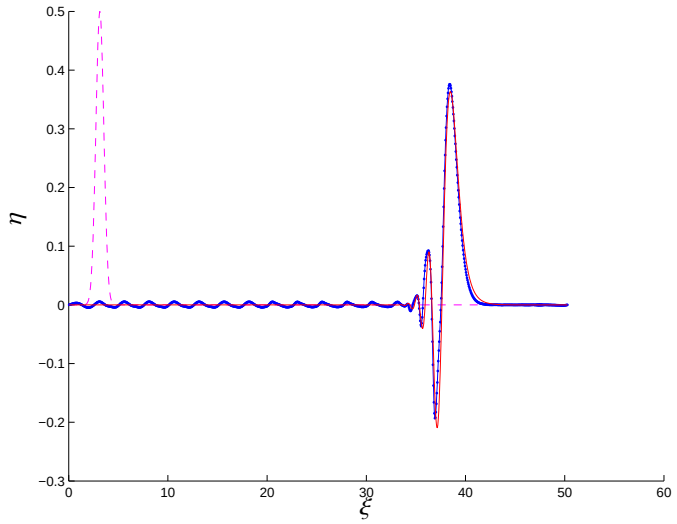


Figure 4.9: Pulse propagating over a synthetic periodic slowly-varying topography. Dotted line: numerical solution for the LCM using RK4 for $t = 36.3247$ and $N = 1024$, dashed line: initial condition, solid line: flat bottom exact solution.

and the initial condition. The other parameters are $\rho_1 = 1$, $\rho_2 = 2$, $N = 1024$, $\Delta\xi = 2\ell/N = 0.0491$, $\Delta t = \Delta\xi = 0.0491$.

A detailed analysis of Fig. 4.9 shows that twice the period of the bottom oscillations (2.5133) is in very good agreement with the reflected wavelength, as expected from Bragg's phenomenon theory [12]. See Fig. 4.10 where vertical bars marking spatial intervals of size 2.5133 fall together with the end of each period of the reflected signal. A comparison between the solutions for the flat and periodic bottoms suggests that the attenuation in the wave amplitude is mainly due to the dispersive term. It is also patent that the oscillations behind the pulse correspond to the reflected wave due to the topography.

**Example 4.5.** The present example adds the nonlinearity ingredient to the previous example. We consider again the periodic slowly-varying coefficient $M(\xi)$

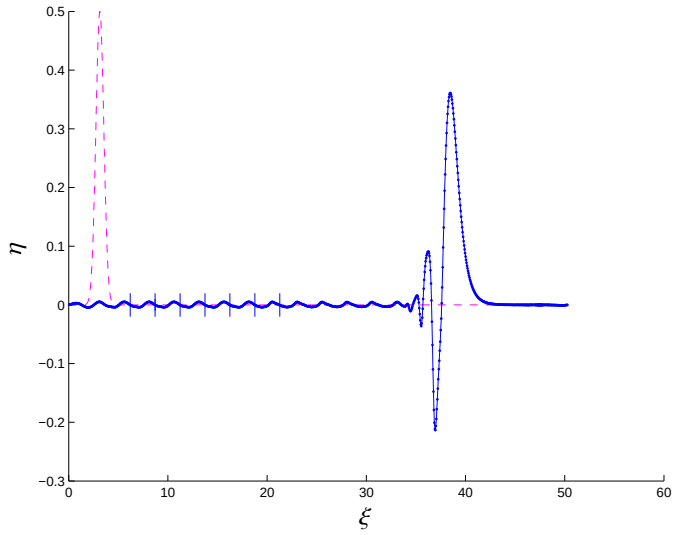


Figure 4.10: Pulse propagating over a synthetic periodic slowly-varying topography. Dashed line: initial condition. Dotted line: numerical solution for the LCM using RK4 for $t = 36.3247$ and $N = 1024$, vertical bars mark spatial intervals of size 2.5133 that fall together with the end of each period of the reflected signal.

defined on the domain $[0, 16\pi]$ as

$$M(\xi) = \begin{cases} 1 + 0.5\sin(5\xi), & \text{for } 6\pi \leq \xi \leq 12\pi, \\ 1, & \text{elsewhere.} \end{cases}$$

The initial perturbation of the interface is the Gaussian function

$$\eta_0(\xi) = 0.5e^{-a(\xi-\pi)^2/64}$$

with $a = 200$ and effective width $L = 2.4$. The ratio inhomogeneities/wavelength is about 0.5236. The physical parameters are $\rho_1 = 1$, $\rho_2 = 2$, $\beta = 0.0001$, $\alpha = 0.01$. We employ $N = 1024$, $\Delta\xi = 2\ell/N = 0.0491$, $\Delta t = \Delta\xi = 0.0491$. In Fig. 4.11 the numerical solution for $t = 32.3977$ is depicted together with the exact solution

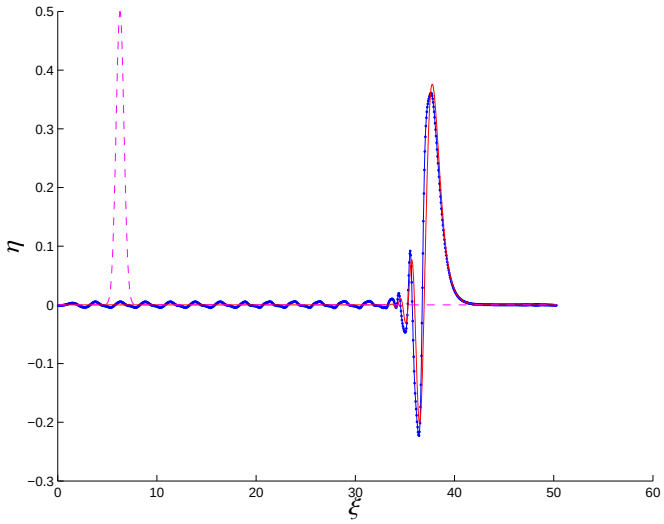


Figure 4.11: Pulse propagating over a synthetic periodic slowly-varying topography. Dotted line: numerical solution for the WNCM using RK4 for $t = 32.3977$ and $N = 1024$, dashed line: initial condition, solid line: exact solution for the LFM.

for the LFM and the initial condition. Again, twice the period of the bottom oscillations (2.5133) is in very good agreement with the reflected wavelength. In Fig. 4.12 vertical bars marking spatial intervals of size 2.5133 fall together with the end of each period of the reflected signal.

**Example 4.6.** Let us consider now a periodic rapidly-varying coefficient $M(\xi)$ defined on the domain $[0, 16\pi]$ as

$$M(\xi) = \begin{cases} 1 + 0.5\sin(15\xi), & \text{for } 6\pi \leq \xi \leq 12\pi, \\ 1, & \text{elsewhere.} \end{cases}$$

The bottom irregularities are located in the region $6\pi \leq \xi \leq 12\pi$. The period of the bottom irregularities is $l = 0.4189$. The initial perturbation of the interface is

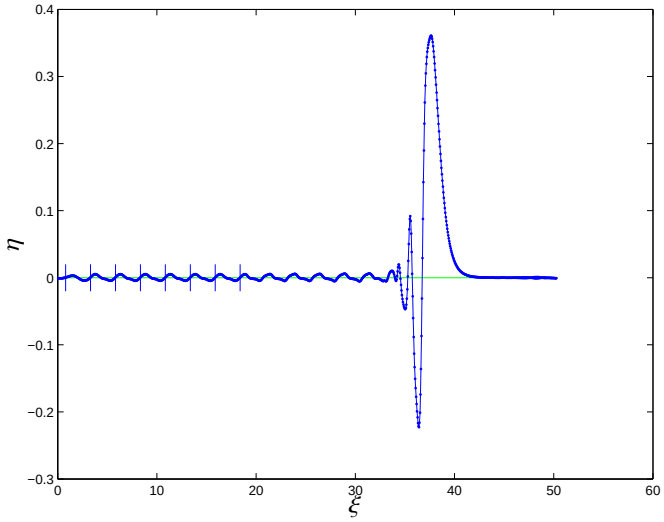


Figure 4.12: Pulse propagating over a synthetic periodic slowly-varying topography. Dotted line: numerical solution for the WNCM using RK4 for $t = 32.3977$ and $N = 1024$, vertical bars mark spatial intervals of size 2.5133 that fall together with the end of each period of the reflected signal.

now the Gaussian function

$$\eta_0(\xi) = 0.5e^{-a(\xi-2\pi)^2/64}$$

with $a = 50$, therefore its effective width is $L = 4.8$ and the ratio inhomogeneities/wavelength is about 0.0873. For the mean velocity $\overline{u_1}$ we choose the corresponding initial condition to ensure one propagation direction for the LFM with $\beta = 0.0001$, $\alpha = 0$, as done in Section 4.3. See Fig. 4.13 where the numerical solution for $t = 35.3429$ is depicted together with the solution for the flat bottom and the initial condition. The other parameters are $\rho_1 = 1$, $\rho_2 = 2$, $N = 1024$, $\Delta\xi = 2\ell/N = 0.049087$, $\Delta t = \Delta\xi = 0.049087$. Note that the solution is very similar to that of the flat bottom case. The wave is not modified by the rapidly-varying topography and no reflections are generated. Only the propagation speed

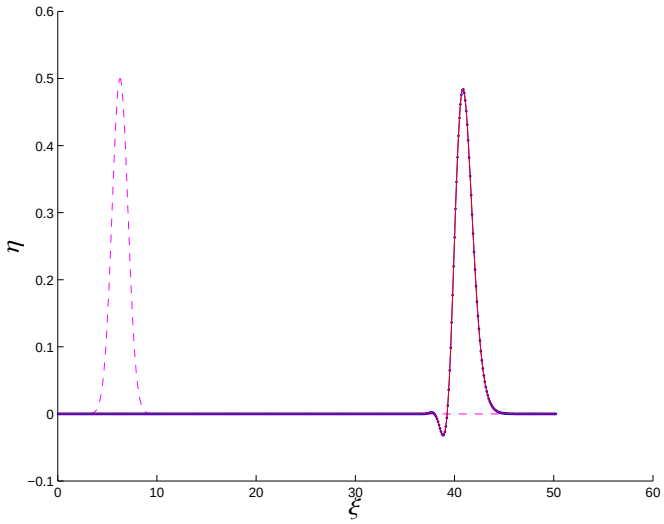


Figure 4.13: Pulse propagating over a synthetic periodic rapid-varying topography. Dotted line: numerical solution for the LCM using RK4 with $N = 1024$ for $t = 35.3429$, dashed line: initial condition, solid line: flat bottom exact solution.

should be slightly decreased as predicted in Rosales and Papanicolaou [26]. But this change is only noticeable over very large distances.

**Example 4.7.** Let us add the nonlinearity ingredient ($\alpha = 0.005$) to the previous example. We consider again the periodic rapidly-varying topography defined in Example 4.6, together with the same Gaussian shape of effective width $L = 4.8$. Therefore the ratio inhomogeneities/wavelength is kept at 0.0873. In Fig. 4.14 the numerical solution for $t = 35.3429$ is depicted together with the exact solution for the LFM and the initial condition. The other parameters are $\beta = 0.0001$, $\rho_1 = 1$, $\rho_2 = 2$, $N = 1024$, $\Delta\xi = 2\ell/N = 0.049087$, $\Delta t = \Delta\xi = 0.049087$. Again, the solution is very similar to that of the LFM. The wave is not modified by the rapidly-varying topography and no reflections are generated.

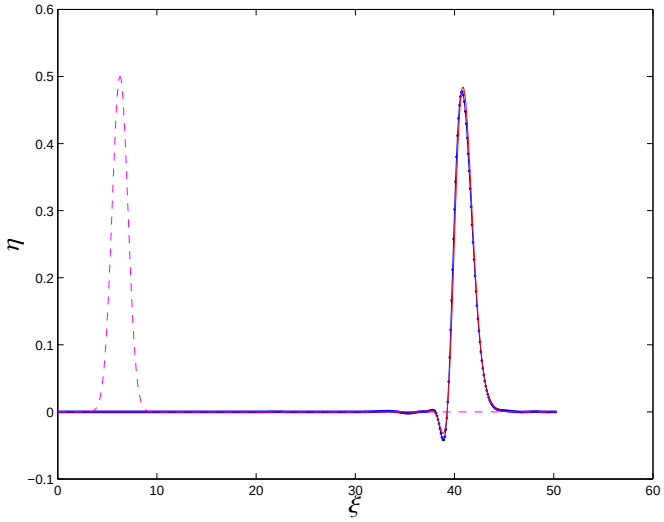


Figure 4.14: Pulse propagating over a synthetic periodic rapid-varying topography. Dotted line: numerical solution for the WNCM using RK4 with $N = 1024$ for $t = 35.3429$, dashed line: initial condition, solid line: flat bottom exact solution.

## 4.5 Computing solitary waves solutions

Now we present two examples of internal solitary waves from the Regularized ILW equation evolving according to the WNFM. That is, we take as initial condition for the WNFM a solitary wave from its unidirectional reduction. We expect the wave to behave almost like a solitary wave. In particular, the balance between nonlinearity and dispersion should be maintained and the wave should travel without a significant change of shape. The velocity of propagation should be similar to that in the ILW equation. The numerical solutions are obtained by the RK4 numerical solver for the WNFM with $\rho_1 = 1$, $\rho_2 = 2$, $\beta = 0.0001$, $\alpha = 0.01$, $N = 256$, $\Delta\xi = 2\ell/N = 0.1963$, $\ell = 8\pi$, $\Delta t = \Delta\xi = 0.1963$.

**Example 4.8.** In Fig. 4.15 the evolution of an approximate solitary wave solution is shown. As initial condition for $\eta$, the parameters $\theta = \pi/8$, $a = -0.09953$

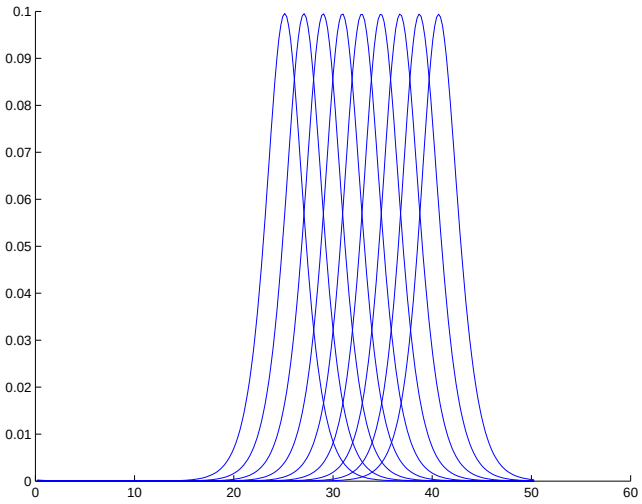


Figure 4.15: Numerical solution of the WNFM with $\beta = 0.0001$, $\alpha = 0.01$ for the propagation of a single solitary wave.

and $\lambda = 0.3323$ are selected in the solitary wave solution of Eq. (2.42); $\overline{u_1}$ is taken to be the corresponding dispersive solution for one propagation direction, see Section 4.3.

The expected behaviour of the wave is captured by the numerical method for long times as shown in Fig. 4.16. The pulse propagates with an approximate velocity of 0.9884 in conformity with its propagation velocity $c = 0.9961$ in the Regularized ILW equation (2.42). The shape of the solitary wave is preserved for long times as shown in Fig. 4.17. The error between the initial condition and the solution that returns to the original position at approximate time $t = 50.8545$ is 0.0047. Taking into account that the choice of $\overline{u_1}$ is an approximation from the linear case ($\alpha = 0$), the result is satisfactory.

**Example 4.9.** In Fig. 4.18 the fission of a single approximate solitary wave solution is simulated. As initial condition for $\eta$, the same parameters $\theta = \pi/8$, $a = -0.099536$ and $\lambda = 0.3323$ are used, while $\overline{u_{10}} = 0$. We observe two waves

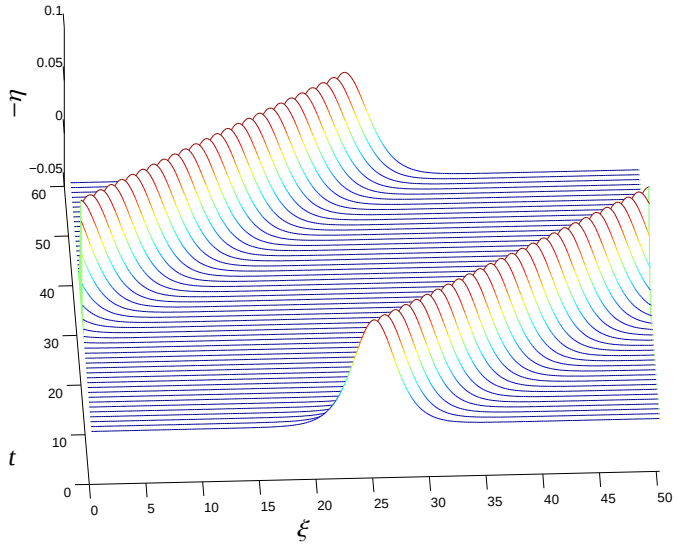


Figure 4.16: Propagation of a single solitary wave until $t = 50.8545$.

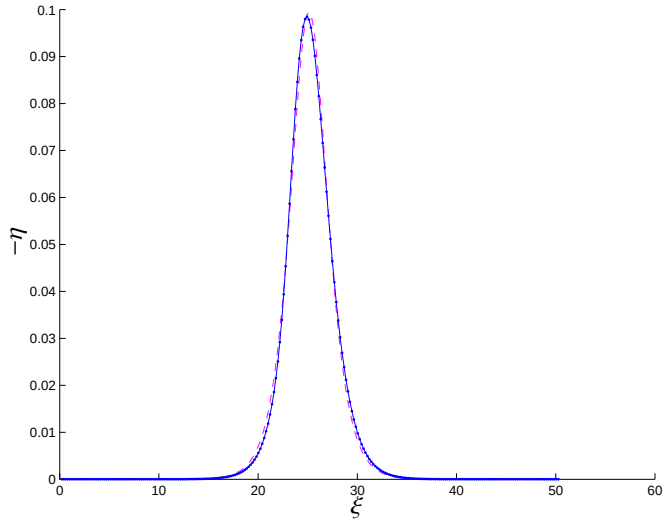


Figure 4.17: A single solitary wave, dashed line: initial condition, dotted line: numerical solution for $t = 50.8545$.

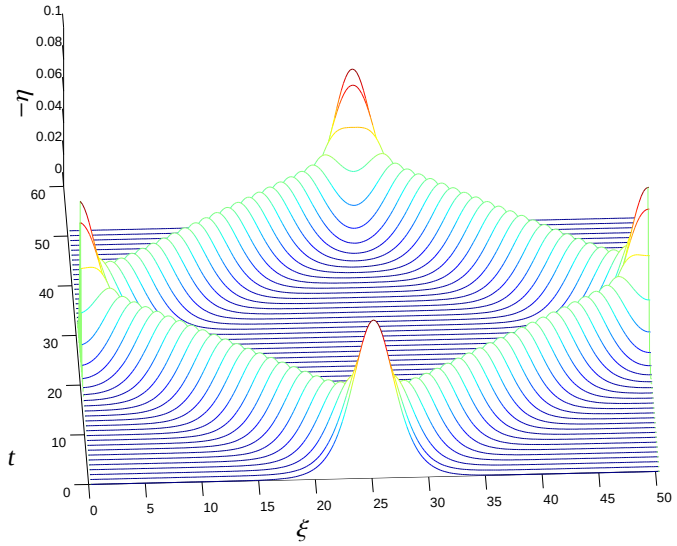


Figure 4.18: Numerical solution of the WNFM for the fission of a single solitary wave.

traveling in opposite directions with approximate speed 0.9846. When they coincide (overlap) in space and time, the initial condition is recovered with an error of $9.8510 \times 10^{-4}$, see Fig. 4.19. This behaviour of the wave is observed for long times as shown in Fig. 4.20.

The examples in this chapter suggest that the model proposed in Chapter 2 can be implemented numerically and that its basic qualitative properties are well captured by the numerical solutions.

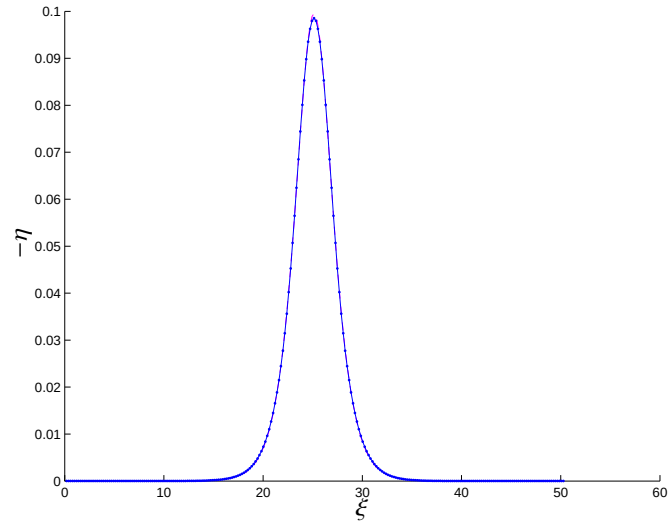


Figure 4.19: Dashed line: initial condition, dotted line: initial wave recovered at $t = 51.0509$, error $= 9.8510 \times 10^{-4}$.

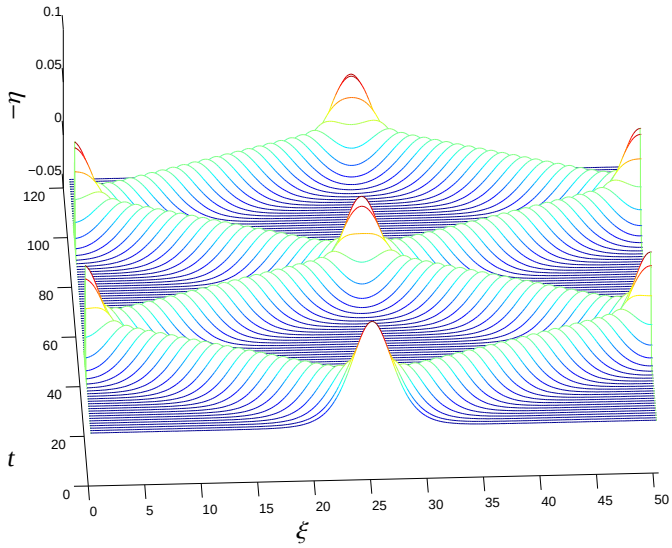


Figure 4.20: Fission of a single solitary wave until $t = 102.1018$.

# Conclusions and future work

In the present work, a one-dimensional strongly nonlinear variable coefficient Boussinesq-type model for the evolution of internal waves in a two-layer system is derived. The regime considered is a shallow water configuration for the upper layer and an intermediate depth for the lower layer. The bottom has an arbitrary, not necessarily smooth nor single-valued profile generalizing the flat bottom model derived in [8]. This arbitrary topography is dealt with by performing a conformal mapping as in [24]. In the unidirectional propagation regime the model reduces to an ILW equation when a slowly varying topography is assumed. The adjustment for the periodic wave case and its computational implementation are also performed. We study the interaction of internal waves with periodic bottom profiles and the evolution of approximate solitary wave solutions. The expected qualitative behaviour is captured. A higher-order reduced one-dimensional model is also obtained, though it has not being implemented computationally yet. Both reduced models have dispersion relations that reproduce correctly the limit from the Euler equations for the shallow water (long waves) regime in the upper layer. The higher-order model, by taking into account the nonhydrostatic correction term for the pressure, approximates better the full dispersion relation. It will be interesting to study numerically the behaviour of the weakly nonlinear higher-order

model regarding this property.

The work initiated here points out some lines of research. We intend to use the strongly nonlinear model and the weakly nonlinear higher order model to study the interaction of large amplitude internal waves with multiscale topography profiles. The refocusing and stabilization of solitary waves for the large levels of nonlinearity allowed by these models is the goal of current research. A difficulty arises to this end, due to the nonlocal dispersive term: it is not easy to find explicit solitary wave solutions for the strongly nonlinear system, and the solitary waves suggested by the weakly one-directional lower-order theory steepen with higher nonlinearity. In [8] the strategy to overcome this difficulty is to use the weakly one-directional solitary wave from the ILW equation as an initial guess for the solitary wave profile. Then find a numerical solitary wave iteratively via the Newton-Raphson method. The profile obtained will serve as initial data for the propagating model.

# Appendix A

# Approximation for the horizontal derivatives at the unperturbed interface

We want to justify the use of $\frac{\sqrt{\beta}}{M(\xi)}\mathcal{T}\left[M(\tilde{\xi})\overline{u_1}_{tx}\right]$ instead of $\left(\frac{\sqrt{\beta}}{M(\xi)}\mathcal{T}\left[M(\tilde{\xi})\overline{u_1}_{t}\right]\right)_x$ in the substitution of $\eta_x$ in system (2.30), in the case of slowly varying topography. Hence we identify $\frac{1}{M(\xi)}\mathcal{T}\left[M(\tilde{\xi})\overline{u_1}_{t}\right]$ as the tangential derivative of the solution of the Laplace equation with Neumann conditions defined in the auxiliary problem

$$\begin{cases} \Phi_{xx} + \Phi_{zz} = 0, & \text{on } -\dfrac{h_2}{L} + \dfrac{h_2}{L}h(\varepsilon x) \le z \le 0, \\ \Phi_z = \overline{u_1}_t, & \text{at } z = 0, \\ \Phi_z - \varepsilon\dfrac{h_2}{L}h'(\varepsilon x)\Phi_x = 0, & \text{at } z = -\dfrac{h_2}{L} + \dfrac{h_2}{L}h(\varepsilon x), \end{cases} \tag{A.1}$$

where $\varepsilon$ is the small parameter defined at the beginning of this text as $L/l$. It was already shown that

$$\Phi_x(x,0,t) = \frac{1}{M(\xi)}\mathcal{T}\left[M(\tilde{\xi})\overline{u_{1t}}\right]$$

via conformal mapping. Now we seek an approximation of $\Phi_{xx}(x,0,t)$, our term of interest, where $t$ is kept frozen. Let $\omega(x,z) = \Phi_x(x,z,t)$. The tangential derivative of $\omega$ at $z = 0$ is our goal. From Eqs. (A.1), $\omega$ satisfies

$$\begin{cases} \omega_{xx} + \omega_{zz} = 0, & \text{on } -\dfrac{h_2}{L} + \dfrac{h_2}{L}h(\varepsilon x) \le z \le 0, \\ \omega_z = \overline{u_1}_{xt}, & \text{at } z = 0, \\ \omega_z - \varepsilon\dfrac{h_2}{L}h'(\varepsilon x)\omega_x - \varepsilon^2\dfrac{h_2}{L}h''(\varepsilon x)\omega = 0, & \text{at } z = -\dfrac{h_2}{L} + \dfrac{h_2}{L}h(\varepsilon x). \end{cases}$$

A conformal mapping taking a flat strip into the corrugated strip above transforms this problem into

$$\begin{cases} \omega_{\xi\xi} + \omega_{\zeta\zeta} = 0, & \text{on } -\dfrac{h_2}{L} \le \zeta \le 0, \\ \omega_\zeta = M(\xi)\,\overline{u_1}_{xt}(\mathrm{x}(\xi,0),t), & \text{at } \zeta = 0, \\ \omega_\zeta - \varepsilon^2\dfrac{h_2}{L}h''(\varepsilon\,\mathrm{x}(\xi,0))\omega = 0, & \text{at } \zeta = -\dfrac{h_2}{L}. \end{cases}$$

Note that a mixed boundary condition (Robin condition) is set on $\zeta = -\frac{h_2}{L}$ instead of a Neumann condition as in all previous problems. Because of the Robin condition, the tangential derivative $\omega_\xi(\xi,0,t)$ is no longer $\mathcal{T}\left[M(\tilde{\xi})\overline{u_1}_{xt}(\mathrm{x}(\tilde{\xi},0),t)\right]$, but it can be approximated by this term up to a certain order in $\varepsilon$. Following a perturbation approach, consider

$$\omega = \omega_0 + \varepsilon\omega_1 + \varepsilon^2\omega_2 + \cdots$$

then $\omega_0$ satisfies the Neumann problem

$$\begin{cases} \omega_{0\xi\xi} + \omega_{0\zeta\zeta} = 0, & \text{on } -\dfrac{h_2}{L} \le \zeta \le 0, \\ \omega_{0\zeta} = M(\xi)\,\overline{u_1}_{xt}(\mathrm{x}(\xi,0),t), & \text{at } \zeta = 0, \\ \omega_{0\zeta} = 0, & \text{at } \zeta = -\dfrac{h_2}{L}, \end{cases}$$

with tangential derivative $\omega_{0\xi}(\xi,0) = \mathcal{T}\left[M(\tilde{\xi})\overline{u_1}_{xt}(\mathrm{x}(\tilde{\xi},0),t)\right](\xi)$. Thus $\omega_{0x} = \omega_{0\xi}/M(\xi)$. The subsequent term is $\omega_1 = 0$ because both boundary conditions are homogeneous to $O(\varepsilon)$. Next $\omega_2$ satisfies

$$\begin{cases} \omega_{2\xi\xi} + \omega_{2\zeta\zeta} = 0, & \text{on } -\dfrac{h_2}{L} \le \zeta \le 0, \\ \omega_{2\zeta} = 0, & \text{at } \zeta = 0, \\ \omega_{2\zeta} - \dfrac{h_2}{L}h''(\varepsilon\,\mathrm{x}(\xi,0))\omega_0 = 0, & \text{at } \zeta = -\dfrac{h_2}{L}. \end{cases}$$

Therefore

$$\omega = \omega_0 + O(\varepsilon^2). \tag{A.2}$$

If we establish a relation between $\alpha$, $\beta$ and $\varepsilon$ of the type $\varepsilon^2 = O(\beta^q)$, with $q \ge \frac{1}{2}$, Eq. (A.2) leads to

$$\left(\frac{1}{M(\xi)}\mathcal{T}\left[M(\tilde{\xi})\overline{u_1}_t\right]\right)_x = \frac{1}{M(\xi)}\mathcal{T}\left[M(\tilde{\xi})\overline{u_1}_{tx}\right] + O\left(\sqrt{\beta}\right),$$

which justifies the approximation done in Eq. (2.39).

# Appendix B

# The Dirichlet-to-Neumann operator

Due to the importance of the Dirichlet-to-Neumann operator ($\mathrm{DtN}_{\mathbf{0}}$) in modelling water waves we pointed here its relation with the Hilbert transform on the flat strip used througout this work.

Given the problem

$$\begin{cases} \mathrm{z}_{\overline{\upsilon}\,\overline{\upsilon}} + \mathrm{z}_{\overline{\omega}\,\overline{\omega}} = 0, & -h \leq \overline{\omega} \leq 0, \\ \mathrm{z}_{\overline{\omega}} = g(\overline{\upsilon}), & \overline{\omega} = 0, \\ \mathrm{z}_{\overline{\omega}} = 0, & \overline{\omega} = -h, \end{cases}$$

the operator $\mathcal{T}$ returns the tangential derivative $\mathrm{z}_{\overline{\upsilon}}(\overline{\upsilon}, 0)$ from the Neumann data $\mathrm{z}_{\overline{\omega}}(\overline{\upsilon}, 0) = g(\overline{\upsilon})$, that is

$$\mathcal{T}[g] = \mathrm{z}_{\overline{\upsilon}}(\overline{\upsilon}, 0).$$

Therefore, its inverse $\overline{\mathcal{T}}$ satisfies

$$g(\overline{\upsilon}) = \mathrm{z}_{\overline{\omega}}(\overline{\upsilon}, 0) = \overline{\mathcal{T}}[\mathrm{z}_{\overline{\upsilon}}(\overline{\upsilon}, 0)]. \tag{B.1}$$

The inverse $\overline{\mathcal{T}}$ of $\mathcal{T}$ has a symbol $-i\tanh(kh)$. Alternatively it can be defined by the principal value integral

$$\overline{\mathcal{T}}[f] = -\frac{1}{2h} \fint \frac{f(v)}{\sinh(\pi(v-\overline{v})/2h)}\, dv. \tag{B.2}$$

The $\mathrm{DtN}_0$ for the problem

$$\begin{cases} \mathrm{z}_{\overline{v}\,\overline{v}} + \mathrm{z}_{\overline{\omega}\,\overline{\omega}} = 0, \quad -h \le \overline{\omega} \le 0, \\ \mathrm{z}(\overline{v}, 0) = f(\overline{v}), \\ \mathrm{z}(\overline{v}, -h) = 0, \end{cases}$$

returns the normal derivative (Neumann condition) from the Dirichlet data. In light of (B.1) we have

$$\mathrm{DtN}_0[f] = \overline{\mathcal{T}}[f'].$$

It means that the Dirichlet-to-Neumann operator applies one differentiation plus the inverse operator $\overline{\mathcal{T}}$ to the Dirichlet data in order to obtain the Neumann condition.

# Appendix C

# The periodic counterpart of the operator $\mathcal{T}$

Due to the nonlocal definition of the Hilbert transform, it is necessary to redefine it when restricting our problem to the periodic domain for numerical implementations. To that end we keep in mind its geometrical interpretation, that is, the operator that takes a harmonic function's normal derivative at the boundary and transforms it into its tangential derivative at the boundary.

Consider the following problem for periodic $\xi \in \Pi[0, 2\ell]$,

$$\begin{cases} \phi_{\xi\xi} + \phi_{\zeta\zeta} = 0, & -h_2/L \leq \zeta \leq 0,\ 0 \leq \xi \leq 2\ell, \\ \phi(0,\zeta) = \phi(2\ell,\zeta), \\ \phi_\zeta(\xi, 0) = g(\xi), \\ \phi_\zeta(\xi, -h_2/L) = 0. \end{cases}$$

Set $\bar{\xi} = \pi\xi/\ell$. In the new coordinates $\bar{\phi}(\bar{\xi}, \zeta) = \phi(\xi, \zeta)$ satisfies

$$\begin{cases} \left(\frac{\pi}{2}\right)^2 \bar{\phi}_{\bar{\xi}\bar{\xi}} + \bar{\phi}_{\zeta\zeta} = 0, \quad -h_2/L \le \zeta \le 0,\ 0 \le \bar{\xi} \le 2\pi, \\ \bar{\phi}(0, \zeta) = \bar{\phi}(2\pi, \zeta), \\ \bar{\phi}_{\zeta}(\bar{\xi}, 0) = \bar{g}(\bar{\xi}), \\ \bar{\phi}_{\zeta}(\bar{\xi}, -h_2/L) = 0. \end{cases} \tag{C.1}$$

We consider the Fourier Series in $\bar{\xi} \in [0, 2\pi]$ with its coefficients given by

$$\begin{aligned} \hat{f}(k) &= \int_0^{2\pi} f(\bar{\xi}) e^{-ik\bar{\xi}}\, d\bar{\xi}, \\ f(\bar{\xi}) &= \frac{1}{2\pi} \sum_{k=-\infty}^{\infty} \hat{f}(k) e^{ik\bar{\xi}}. \end{aligned} \tag{C.2}$$

The Discrete Fourier Transform (DFT) in $\bar{\xi}$ is

$$\hat{f}(k) = \Delta\bar{\xi} \sum_{j=1}^{N} f(\bar{\xi}_j) e^{-ik\bar{\xi}_j}, \quad \bar{\xi}_j = j\Delta\bar{\xi}, \quad \Delta\bar{\xi} = \frac{2\pi}{N},$$

exactly the same one used by Trefethen [28] together with the inverse

$$f(\bar{\xi}_j) = \frac{1}{2\pi} \sum_{k=-N/2+1}^{N/2} \hat{f}(k) e^{ik\bar{\xi}_j}, \quad j = 1, \ldots, N,$$

where $k \in \{-N/2 + 1, \ldots, N/2\}$ because in the discrete domain $e^{ikj\Delta\bar{\xi}} = e^{ikj2\pi/N}$ so there is no difference for $k = k_0 \bmod N$.

Apply the Fourier Transform to problem (C.1):

$$\begin{cases} (-ik)^2 \left(\frac{\pi}{\ell}\right)^2 \hat{\bar{\phi}} + \hat{\bar{\phi}}_{\zeta\zeta} = 0, \quad \text{on } -h_2/L \le \zeta \le 0, \\ \hat{\bar{\phi}}_{\zeta}(k,0) = \hat{\bar{g}}(k), \\ \hat{\bar{\phi}}_{\zeta}(k,-h_2/L) = 0. \end{cases} \tag{C.3}$$

The solution for problem (C.3) is

$$\hat{\bar{\phi}}(k,\zeta) = \frac{\hat{\bar{g}}(k)}{\pi k/\ell} \frac{\cosh\left(\frac{k\pi}{\ell}\left(\zeta + \frac{h_2}{L}\right)\right)}{\sinh\left(\frac{k\pi}{\ell}\frac{h_2}{L}\right)}, \quad k \neq 0.$$

Therefore, for $C^1$ initial Neumann data $g$,

$$\begin{aligned} \bar{\phi}(\bar{\xi},\zeta) &= \frac{1}{2\pi} \sum_{k=-\infty}^{\infty} \hat{\bar{\phi}}(k,\zeta) e^{ik\bar{\xi}}, \\ &= \frac{1}{2\pi} \sum_{\substack{k=-\infty \\ k\neq 0}}^{\infty} \frac{\hat{\bar{g}}(k)}{\pi k/\ell} \frac{\cosh\left(\frac{k\pi}{\ell}\left(\zeta + \frac{h_2}{L}\right)\right)}{\sinh\left(\frac{k\pi}{\ell}\frac{h_2}{L}\right)} e^{ik\bar{\xi}} + \frac{\hat{\bar{\phi}}(0)}{2\pi}, \end{aligned}$$

the convergence is uniform in $0 \le \bar{\xi} \le 2\pi$ and also in $-h_2/L \le \zeta \le 0$ since

$$\left| \frac{\cosh\left(\frac{k\pi}{\ell}\left(\zeta + \frac{h_2}{L}\right)\right)}{\sinh\left(\frac{k\pi}{\ell}\frac{h_2}{L}\right)} \right| \le \left| \frac{\cosh\left(\frac{k\pi}{\ell}\frac{h_2}{L}\right)}{\sinh\left(\frac{k\pi}{\ell}\frac{h_2}{L}\right)} \right| = \left| \coth\left(\frac{\pi}{\ell}\frac{h_2}{L}\right) \right|, \tag{C.4}$$

for all integer $k \neq 0$.

We want $\phi_\xi$; returning to the original variables

$$\phi(\xi,\zeta) = \frac{1}{2\pi} \sum_{\substack{k=-\infty \\ k\neq 0}}^{\infty} \frac{\hat{\bar{g}}(k)}{\pi k/\ell} \frac{\cosh\left(\frac{k\pi}{\ell}\left(\zeta + \frac{h_2}{L}\right)\right)}{\sinh\left(\frac{k\pi}{\ell}\frac{h_2}{L}\right)} e^{ik\xi\pi/\ell} + \frac{\hat{\bar{\phi}}(0)}{2\pi}.$$

Taking $\xi$-derivatives,

$$\phi_\xi(\xi,\zeta) = \frac{1}{2\pi}\sum_{\substack{k=-\infty\\k\neq 0}}^{\infty} \hat{\bar{g}}(k)\frac{i\cosh\left(\frac{k\pi}{\ell}\left(\zeta+\frac{h_2}{L}\right)\right)}{\sinh\left(\frac{k\pi}{\ell}\frac{h_2}{L}\right)}e^{ik\xi\pi/\ell}.$$

The tangential derivative at the boundary is obtain making $\zeta \to 0$:

$$\phi_\xi(\xi,0) = \frac{1}{2\pi}\sum_{\substack{k=-\infty\\k\neq 0}}^{\infty} \hat{\bar{g}}(k)\frac{i\cosh\left(\frac{k\pi}{\ell}\frac{h_2}{L}\right)}{\sinh\left(\frac{k\pi}{\ell}\frac{h_2}{L}\right)}e^{ik\xi\pi/\ell}.$$

The convergence is still uniform because of Eq. (C.4).

Therefore,

$$\mathcal{T}_{[0,2\ell]}[f](\xi) = \frac{1}{2\pi}\sum_{\substack{k=-\infty\\k\neq 0}}^{\infty} i\coth\left(\frac{k\pi}{\ell}\frac{h_2}{L}\right)e^{ik\xi\pi/\ell}\,\hat{\bar{f}}(k),$$

where

$$\hat{\bar{f}}(k) = \int_0^{2\pi}\bar{f}(\bar{\xi})e^{-ik\bar{\xi}}\,d\bar{\xi}, \quad \bar{\xi} = \pi\xi/\ell,$$

that is, the Fourier coefficients in $\Pi[0,2\pi]$.

It is also convenient to write the composition of one spatial derivative with the Hilbert transform $\mathcal{T}_{[0,2\ell]}[\cdot]$ because they always come together in the models considered here,

$$\mathcal{T}_{[0,2\ell]}[f]_\xi(\ell\bar{\xi}/\pi) = \frac{1}{2\pi}\sum_{\substack{k=-\infty\\k\neq 0}}^{\infty} -\frac{k\pi}{\ell}\coth\left(\frac{k\pi}{\ell}\frac{h_2}{L}\right)e^{ik\bar{\xi}}\,\hat{\bar{f}}(k).$$

Finally, for the discretization of the periodic domain (ignoring the aliasing

effect) we have that

$$\mathcal{T}_{[0,2\ell]}[f]_{\xi}(\bar{\xi}_j) \approx \frac{1}{2\pi} \sum_{\substack{k=-N/2+1 \\ k\neq 0}}^{N/2} -\frac{k\pi}{\ell} \coth\left(\frac{k\pi}{\ell}\frac{h_2}{L}\right) e^{ik\bar{\xi}_j}\, \hat{\bar{f}}(k), \qquad j = 1, \ldots, N,$$

where

$$\hat{\bar{f}}(k) = \Delta\bar{\xi} \sum_{j=1}^{N} \bar{f}(\bar{\xi}_j) e^{-ik\bar{\xi}_j}.$$

In conclusion, the symbol of the operator $\mathcal{T}_{[0,2\ell]}[\cdot]_{\xi}$ (that is the composition of one spatial derivative with the Hilbert transform) in the new coordinate $\bar{\xi}$ is

$$-\frac{k\pi}{\ell} \coth\left(\frac{k\pi}{\ell}\frac{h_2}{L}\right).$$

# Bibliography


[1] Artiles, W. & Nachbin, A., 2004. “Nonlinear evolution of surface gravity waves over highly variable depth,” *Physical Review Letters*, vol. 93, pp. 234501–1–234501–4.

[2] Ascher, U. M. & Petzold, L. R., 1988. *Computer Methods for Ordinary Differential Equations and Differential–Algebraic Equations*, SIAM.

[3] Benjamin, T. B., 1967. “Internal waves of permanent form of great depth,” *Journal of Fluid Mechanics*, vol. 29, pp. 559–592.

[4] Benjamin, T. B., Bona, J. L. & Mahony, J. J., 1972. “Model equations for long waves in nonlinear dispersive systems,” *Philosophical Transactions of the Royal Society of London. Series A, Mathematical and Physical Sciences*, vol. 272, No. 1220, pp. 47–78.

[5] Camassa, R. & Levermore, C. D., 1997. “Layer-mean quantities, local conservation laws, and vorticity,” *Physical Review Letters*, vol. 78, pp. 650–653.

[6] Choi, W., & Camassa, R., 1996. “Long internal waves of finite amplitude,” *Physical Review Letters*, vol. 77, pp. 1759–1762.

[7] Choi, W., & Camassa, R., 1996. “Weakly nonlinear internal waves in a two-fluid system,” *Journal of Fluid Mechanics*, vol. 313, pp. 83–103.

[8] Choi, W., & Camassa, R., 1999. “Fully nonlinear internal waves in a two-fluid system,” *Journal of Fluid Mechanics*, vol. 396, pp. 1–36.

[9] Davis, R. E., & Acrivos, A., 1967. “Solitary internal waves in deep water,” *Journal of Fluid Mechanics*, vol. 29, pp. 593–607.

[10] Driscoll, T., *Schwarz-Christoffel toolbox for Matlab*, `http://www.math.udel.edu/~driscoll/software`.

[11] Green, A. E. & Naghdi, P. M., 1976. “A derivation of equations for wave propagation in water of variable depth,” *Journal of Fluid Mechanics*, vol. 78, pp. 237–246.

[12] Guazzeli, E., Rey, V. & Belzons, M., 1992. “Higher order Bragg reflection of gravity surface waves by periodic beds,” *Journal of Fluid Mechanics*, vol. 245, pp. 301–317.

[13] Jo, T.-C. & Choi, W., 2002. “Dynamics of strongly nonlinear internal solitary waves in shallow water,” *Studies in Applied Mathematics*, vol. 109, pp. 205–227.

[14] Joseph, R. I., 1977. “Solitary waves in finite depth fluid,” *Journal of Physics* A, vol. 10, pp. L225–L227.

[15] Keener, J. P., 2000. *Principles of Applied Mathematics: Transformation and Approximation*, Westview Press.

[16] Koop, C. G. & Butler, G., 1981. “An investigation of internal solitary waves in a two-fluid system,” *Journal of Fluid Mechanics*, vol. 112, pp. 225–251.

[17] Kubota, T., Ko, D., & Dobbs, L., 1978. “Propagation of weakly non linear internal waves in a stratified fluid of finite depth,” *AIAA Journal Hydrodynamics*, vol. 12, pp. 157–165.

[18] Lamb, H., 1932. *Hydrodynamics*, Dover.

[19] Matsuno, Y., 1992. “Nonlinear evolutions of surface gravity waves on fluid of finite depth,” *Physical Review Letters*, vol. 69, pp. 609–611.

[20] Matsuno, Y., 1993. “A unified theory of nonlinear wave propagation in two-fluid systems,” *Journal of the Physical Society of Japan*, vol. 62, pp. 1902–1916.

[21] Muñoz, J. C. & Nachbin, A., 2004. “Dispersive wave attenuation due to orographic forcing,” *SIAM Journal of Applied Mathematics*, vol. 64, Issue 3, pp. 977–1001.

[22] Muñoz, J. C. & Nachbin, A., 2005. “Stiff microscale forcing and solitary wave refocusing,” *SIAM Multiscale Modeling and Simulation*, vol. 3, issue 3, pp. 680–705.

[23] Muñoz, J. C. & Nachbin, A., 2006. “Improved Boussinesq-type equations for highly-variable depths,” *IMA Journal of Applied Mathematics*, vol. 71, pp. 600–633.

[24] Nachbin, A., 2003. “A terrain-following Boussinesq system,” *SIAM Journal on Applied Mathematics*, vol. 63, pp. 905–922.

[25] Ono, H., 1975. “Algebraic solitary waves in stratified fluids,” *Journal of the Physical Society of Japan*, vol. 39, pp. 1082–1091.

[26] Rosales, R. R. & Papanicolaou, G. C., 1983. “Gravity waves in a channel with a rough bottom,” *Studies in Applied Mathematics*, vol. 68, pp. 89–102.

[27] Su, C. H. & Gardner, C. S., 1969. “Korteweg-de Vries Equation and Generalizations. III. Derivation of the Korteweg-de Vries Equation and Burgers Equation,” *Journal of Mathematical Physics*, vol. 10, issue 3, pp. 536–539.

[28] Trefethen, L. N., 2000. *Spectral Methods in Matlab*, SIAM.

[29] Wei, G. & Kirby, J., 1995. “Time-dependent numerical code for extended Boussinesq equations,” *Journal of Waterway, Port, Coastal and Ocean Engineering*, vol. 121 pp. 251–261.

[30] Whitham, G. B., 1974. *Linear and nonlinear waves*, John Wiley, New York–London–Sidney.

[31] Wu, T. Y., 1981. “Long waves in ocean and coastal waters,” *Journal of the Engineering Mechanics Division ASCE*, vol. 107, No. 3, pp. 501–522.